电 化 学
J. Electrochem. 2022, 28(2), 2108501 (1 of 25)

【Review】 **DOI**: 10.13208/j.electrochem.210850 **Http**://electrochem.xmu.edu.cn

Recent Advances in Structural Regulation on Non-Precious Metal Catalysts for Oxygen Reduction Reaction in Alkaline Electrolytes

Xue Wang[1,2], Li Zhang[1], Chang-Peng Liu[1,2], Jun-Jie Ge[1,2], Jian-Bing Zhu[1,2*], Wei Xing[1,2*]

(*1. State Key Laboratory of Electroanalytical Chemistry, Changchun Institute of Applied Chemistry, Chinese Academy of Sciences, Changchun 130022, Jilin, China; 2. University of Science and Technology of China, Hefei 230026, Anhui, China*)

Abstract: Oxygen reduction reaction (ORR) in alkaline electrolytes is an important electrochemical process for metal-air batteries and anion exchange membrane fuel cells (AEMFCs). However, the sluggish kinetics spurs intensive research on searching robust electrocatalysts. Non-precious metal catalysts (NPMCs) that can circumvent the cost and scarcity issues associated with platinum (Pt)-based materials have been pursued and the challenges lie in the performance improvement to rival Pt-based benchmarks. As the composition and structure of the NPMCs have a significant impact on the catalytic performance, precise regulation on the catalyst structure holds great promise to bridge the activity gap between NPMCs and Pt-based benchmarks. In this minireview, we aim to provide an overview of recent progress in the structural regulation on NPMCs towards improved performance. The four typical categories of NPMCs, i.e., metal-free carbon-based materials, metal compounds, metal encapsulated in graphitic layer and atomically dispersed metal-nitrogen-carbon materials, are firstly introduced, where catalytic active sites and catalytic mechanism are highlighted. Subsequently, we summarize the representative structural regulation from a nanoscale to an atomic scale including hierarchically porous structure regulation, interface engineering, defect engineering and atomic pair construction. Special emphasis is placed on the elucidation of the catalytic structure-performance relationship. The origins of activity improvements from these structural regulations are discussed in terms of accelerated mass transfer, increased accessible active sites, tailored electronic states, and synergetic effect between multi-components. Finally, the challenges and opportunities are discussed.

Key words: oxygen reduction reaction; non-precious metal catalysts; structural regulation

1 Introduction

In response to energy crisis and environmental pollution, searching for sustainable and renewable energy sources has become an important mission of modern chemistry[1]. In this context, a variety of clean energy conversion and storage technologies, i.e., anion exchange membrane fuel cells (AEMFCs)[2] and metal-air batteries[3], have attracted extensive research interes ts. The practical employment of these sustainable energy technologies, however, is greatly obstructed by the sluggish kinetics of key electrocatalytic reaction, oxygen reduction reaction (ORR) at a cathode[4]. Therefore, efficient electrocatalysts are necessitated to accelerate ORR toward improved conversion efficiency. Generally, ORR proceeds through either a direct four-electron reduction to OH^- or an indirect two-electron pathway to HO_2^- (Table 1). Due to the higher energy-conversion efficiency and suppressed poison-

Cite as: Wang X, Zhang L, Liu C P, Ge J J, Zhu J B, Xing W. Recent advances in structural regulation on non-precious metal catalysts for oxygen reduction reaction in alkaline electrolytes. *J. Electrochem.*, 2022, 28(2): 2108501.

Received: 2021-11-01, Revised: 2021-12-02. *Corresponding author,Tel: (86-431)85262147, E-mail: zjb@ciac.ac.cn; xingwei@ciac.ac.cn

ing effect induced by HO_2^-, the direct four-electron pathway is always pursued [5,6]. Although, platinum (Pt)-based materials are recognized as the most efficient one in terms of activity and selectivity, but the high cost and limited reserves impede the widespread commercialization. Motivated by these challenges, developing non-precious metal catalysts (NPMCs) that feature with comparable activity for ORR as the Pt-based ones represents the core of these electrochemical energy conversion and storage technologies[7-9]. The past decades have witnessed a boom in the diversity of NPMCs from metal-free carbons to transition metal-based materials, accompanied by the active site transition from carbon to metal and thus the enhancement in catalytic performance. In 2009, Dai and co-workers[10] reported the first demonstration of vertically aligned nitrogen-doped carbon nanotubes (VA-NCNTs) as metal-free ORR catalysts. Pioneered by this work, substantial attempts have been made to develop advanced metal-free heteroatoms doped carbon catalysts[11-13]. A parallel effort has been devoted to metal compounds since Dai's group[14] first discovered a hybrid material consisting of Co_3O_4 nanocrystals grown on reduced graphene oxide as a high-performance ORR catalyst arising from synergistic chemical coupling effects between Co_3O_4 and graphene, there is a stronger ionic Co-O bonding in the hybrid. Density functional theory (DFT) calculations manifest that the charge transfer from graphene to Co_3O_4 improves the electronic conductivity of the overall structure, thereby improving the ORR performance[15]. Another unique metal-carbon interface electronic interaction was found by Bao and co-workers in 2013 [16], which leads to a new family of NMPMs, metals or metal carbides encapsulated in graphitic layer. Apart from these heterogenous structured catalysts, atomically dispersed metal-nitrogen-carbon (M-N-C) materials that combine the merits of both heterogenous and homogeneous catalysts are capturing increasing attention and hailed as a new frontier in the field[17-19].

Beyond the category diversity and performance enhancement, increasing efforts are paid on the understanding of the structure-activity relationship, which is beneficial for the rational structure regulation on electrocatalysts to obtain desirable catalytic behaviours. In recent years, structural regulation on the electrocatalysts from a microscale to an atomic scale is recognized as one of the most powerful strategies to bridge the activity gap between NPMCs and Pt-based benchmarks[20-22]. For example, building a hierarchically porous architecture is favorable to guarantee sufficient active site density and smooth electron/mass transportation towards dramatically boosted performance. Engineering the interface structure of the heterogenous electrocatalysts is also effective to modify the electrocatalytic properties by synergetic effect and/or electronic interaction between different components. Beyond that, exquisitely manipulating the active site structure at an atomic scale is hailed as the most direct approach to regulate the performance through short-range electronic modulation effect. A timely summary of the current advancements and future perspectives for further investigation is urgently desirable in ORR community and beyond.

In this minireview, structural regulation strategies for the representative NPMCs are systematically summarized. Firstly, we give a general introduction of the four typical categories of NPMCs, namely, metal-free heteroatoms doped carbon materials, metal compounds, transition-metals encapsulated in graphitic layers, and the atomically dispersed M-N-C materials, with the emphasis on the structure-activity relationship understanding for the different catalyst families. Subsequently, structural regulation strategies towards improved catalytic properties of these NPMCs are discussed in detail regarding pore design, interface engineering, defect engineering and atomic pair site construction. In this section, the important role of microenvironment on the electronic structure with the resultant catalytic properties is highlighted. Finally, we present an outlook particularly on the trend and challenges of the structural regulation from a nanoscale to an atomic scale.

2 Catalyst Materials

2.1 Metal-Free Carbon-Based Materials

The development of metal-free carbon-based ma-

Table 1 Reaction equations of ORR in alkaline conditions.

Mechanism			Overall reaction
Four-electron process	Dissociation pathway	$O_2 + 2* \rightarrow 2O*$ $2O* + 2e^- + 2H_2O \rightarrow 2OH* + 2OH^-$ $2OH* + 2e^- \rightarrow 2OH^- + 2*$	$O_2 + 2H_2O + 4e^- \rightarrow 4OH^-$
	Associative pathway	$O_2 + * \rightarrow O_2*$ $O_2* + H_2O + e^- \rightarrow OOH* + OH^-$ $OOH* + e^- \rightarrow O* + OH^-$ $O* + H_2O + e^- \rightarrow OH* + OH^-$ $OH* + e^- \rightarrow OH^- + *$	
Two-electron process		$O_2 + * \rightarrow O_2*$ $O_2* + H_2O + e^- \rightarrow OOH* + OH^-$ $OOH* + e^- \rightarrow HO_2^- + *$	$O_2 + H_2O + 2e^- \rightarrow HO_2^- + OH^-$

terials for ORR experienced three stages: non-doped defective carbon materials, single heteroatom doped carbons and multi-heteroatoms doped carbons. The intrinsic defects, i.e., vacancy, pentagon carbon ring, and Stone-Wales defects, would break the symmetry of the charge density distribution towards localized π electrons, thereby promoting oxygen adsorption and the subsequent electron transfer process. For example, a single vacancy was reported to increase charge density of the carbon atoms located at the zigzag edge by 0.02 e[23]. And the catalytic active sites usually locate at the zigzag edge or at the end of the pentagon-pentagon-octagon chains. In an attempt to clarify the major active site, highly oriented pyrolytic graphite catalyst with specific pentagon carbon defective patterns was employed (Figure 1)[24]. Combining work-function analyses with macro and micro-electrochemical performance measurements, the dominated active site was determined as pentagon defects. However, the ORR activity of the non-doped carbon materials lags far behind that of the Pt-based benchmarks and the ORR always proceeds through an undesirable two-electron pathway[25].

Theoretical calculations show that the adsorption and reduction of O_2 molecules can be facilitated by doping heteroatoms into graphite substrate[26]. This is because doping can redistribute charge density and/or spin density of inert carbons towards regulated work function as a result of electronegativity difference between heteroatoms and carbon atoms. Nitrogen (N) is the most widely used dopants and the activity is found to be correlated with doping level and type of nitrogen species. Earlier work[27] suggests that graphitic/quaternary N contributes to the majority of the ORR catalytic activities because it can break the symmetry electron distribution and thus facilitating oxygen adsorption. While recent studies[28,29] imply the crucial role of pyridinic N as it can activate the adjacent carbon atoms. By contrast, Ding et al.[30] highlighted the importance of pyridinic/pyrrolic N on the ORR activity and selectivity. In order to preferential doping pyridinic/pyrrolic N into a carbon substrate, our group[31] employed the nano-$CaCO_3$ template to generate edge defects by the *in-situ* released CO_2 gas. With a large number of pyridinic/pyrrolic N formed at these defect sites, the catalyst exhibits high ORR selectivity with the number of transferred electrons calculated to be 3.7 ~ 3.8 from the K-L plots.

Compared with the single heteroatom doping, multi-doping is proven to be more effectively tailoring the catalytic properties due to the synergy effect. N and sulfur (S) co-doped, and N and phosphor (P) co-doped carbon materials are extensively studied[32-34]. For example, our group[34] reported the high-performance N, S co-doped carbon materials, and investigated the synergy between N and S. The doping level can be well controlled by pre-oxidizing the carbon-based surface prior to S doping (Figure 2(A)). The results show that the ORR activity is highly depended on the pyridinic N and C-S-C contents. S-doping can increase

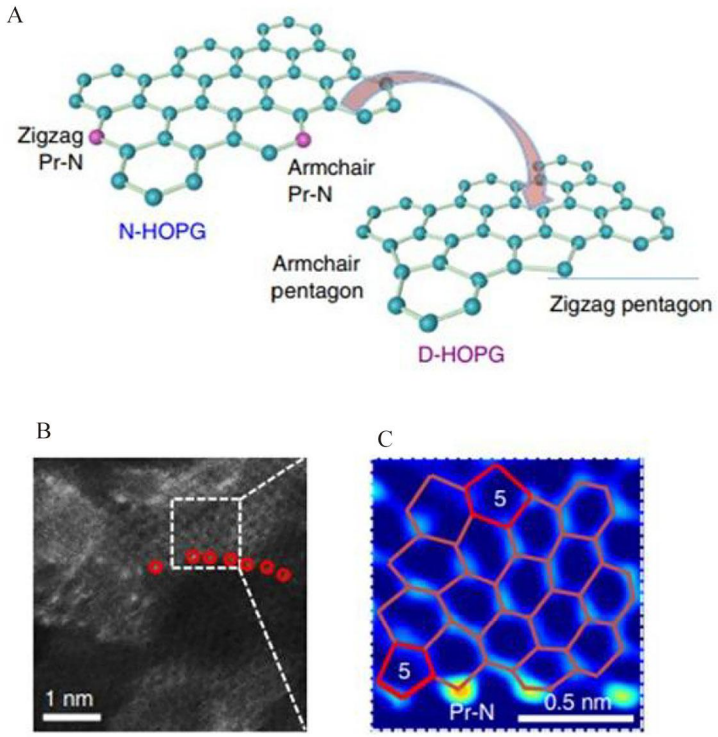

Figure 1 (A) Illustration of the edge defect reconstruction; (B) The HAADF-STEM image of N-G. The nitrogen atoms are marked with the red circles; (C) Expanded image of the dotted box in (B) ('5' indicates the pentagons). Reproduced with permission of Ref. 24, copyright 2019 Springer Nature. (color on line)

the spin density of the surrounding C atoms[35], while N dopants can afford the surrounding C atoms with moderate positive charge, such that the presence of C-S-C lowers the energy barrier for the first electron transfer step compared with N doped carbon, and leads to the enhanced intrinsic activity. (Figure 2(B) and 2(C)). Compared with dual atoms doping, tri-atoms doping can further enhance the asymmetry of the spin density of carbon and the degree of sp^2-C, thereby improving the catalytic activity and conductivity of the material. In a recent report from Yu' group[36], introducing additional P into N, S co-doped reduced graphene oxide (rGO) realized a 2-fold activity enhancement compared with the original N, S-rGO. The activity improvement was supposed to stem from the so-called synergy between these dopants, i.e., increased active site density, higher intrinsic activity and improved conductivity. For example, the N-P species were regraded to affect the band gap of the catalytic material, which increases the charge-carrier density of carbon. On the basis of N, S-C, in addition to doping with P, doping with oxygen (O) can also achieve improved ORR activity. Take the work from Yang's group[37] as an example, a novel N, S, O tri-doped carbon nanosheet catalyst was prepared. And the amount of O dopants in the carbon substrate is controlled by altering the content of colloidal silica. With the increase in the content of silica, the content of O is increased, resulting in the activity enhancement.

At present, doping various non-metallic elements into carbon materials has become an effective way to improve ORR activity. However, their performance is still inferior to the metal-based ones and the Pt-based benchmarks. Thus, for these metal-free carbon-based materials, which calls for the rational design of the multi-scale structures, i.e., morphology, active site structure to regulate the site density and intrinsic activity simultaneously.

2.2 Metal Compounds

In addition to carbon-based materials, transition metal compounds including oxides[14,38,39], phosphides[40-42],

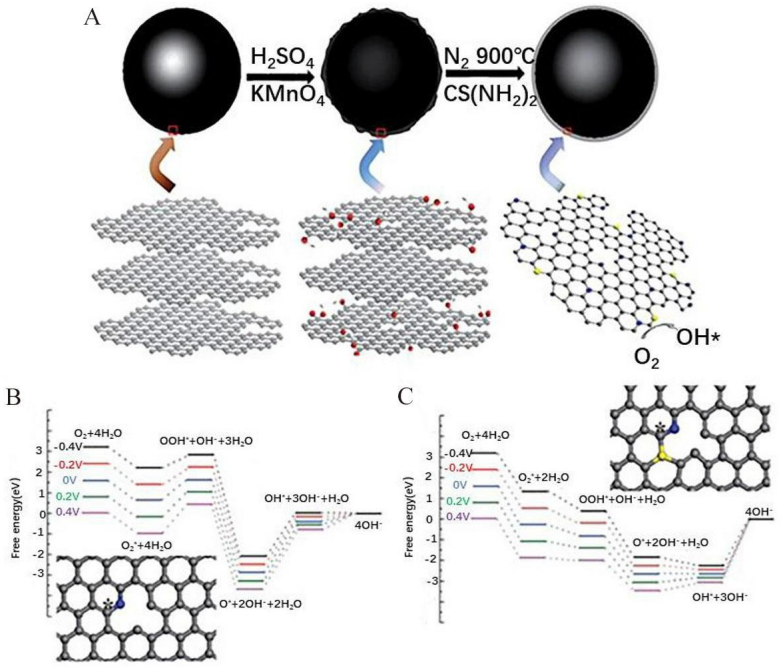

Figure 2 (A) Schematic illustration showing the synthesis of N, S co-doped carbon catalysts; (B, C) Free-energy diagrams of the ORR mechanism at different electrode potentials (U) on (B) N doped carbon and (C) N, S co-doped carbon. The * denotes the free C site on doped carbon structure. Insets: the optimized structure of N doped and N, S co-doped carbon structure. The gray, blue and yellow balls denote C, N and S, respectively. Reproduced with permission of Ref. 34, copyright 2016 Royal Society of Chemistry. (color on line)

sulfides[43], carbides[44-46], nitrides[47-49] and corresponding composite materials[50] have become another promising ORR catalysts due to their relatively low price, high abundance and nonpoisonous to environments. Specifically, perovskite-type oxides that own flexible and controllable structure by changing the content of doping elements to regulate the strength of the metal-oxygen bond are one of the most promising alternatives. Du et al.[39] doped $LaCoO_3$ with an appropriate amount of Mn to regulate the e_g orbital-filling electrons. Besides, the content of O vacancy and the O 2p orbital energy level increased, thus reinforcing the covalency of the Co-O bond. These adjustments were conducive to improve ORR activity towards the apex of the volcanic curve. Similarly, optimizing the filling number of e_g orbitals by doping Fe in $LaCoO_3$ leads to the enhanced degree of hybridization of Co 3d and O 2p orbitals, which is beneficial for activity improvement[51]. Beyond the perovskite-type oxides, transition metal oxides coupled with carbon supports represent another promising catalyst family as MnO_2 deposited onto 3D Vertically Aligned Carbon Nanotube Array (VACNTs-MnO_2) composites[38], Co_3O_4 nanocrystals coupled with N-doped reduced graphene oxide[14] show excellent ORR activity.

Metal phosphides with high conductivity are also explored as ORR catalysts. P has higher electronegativity and can attract electrons from metals, which serves as a Lewis base to work with positively charged protons during the ORR process. Xu and co-workers[41] synthetized Co_2P embedded in Co, N, and P multi-doped carbon material by one-step phosphidation. During the pyrolysis process, Co^{2+} is reduced to metallic Co, sequentially reacts with P steam to produce Co_2P. DFT calculation demonstrated a relatively higher Fermi level and the d-band center for Co_2P than the metallic Co, suggesting remarkable electronic transfer from Co to P, which may be favorable for adsorption of ORR intermediates. The bimetallic NiCo-P[52], and trimetallic FeNiCo-P[40], by contrast, show enhanced activity than single metal. Ren et al.[40] prepared the well-designed hierarchically porous N-doped nanorod

loaded with Fe-Ni-Co trimetal/trimetal phosphide nanoparticles (FeNiCo@NC-P), in which Co is the mainly active site for ORR, while Fe/Ni predominantly serve as active sites for oxygen evolution reaction (OER). Besides, the electronic modulation effect between these components was supposed to further improve their intrinsic activity. Consequently, the integrated FeNiCo@NC-P catalyst exhibited enhanced bifunctional ORR and OER performance.

As the analogue to metal oxides, metal sulfides attract considerable research attention as well. Deng's group[53] integrated $NiCo_2S_4$ with graphitic carbon nitride carbon nanotube ($NiCo_2S_4$@g-C_3N_4-CNT). Due to the intrinsic property of $NiCo_2S_4$ and the strong interaction with support, the ORR kinetics are significantly accelerated. In order to further improve the electronic interaction with support, graphene quantum dots can be introduced into bimetallic $NiCo_2S_4$ by Liu et al.[54], which is realized by NiCo-based carbonate hydroxides growth, sulfuration process and electrophoretic deposition (Figure 3(A)). It is worth noting that the current density of N-GQDs/$NiCo_2S_4$/CC composite catalyst at 0.8 V only emerged negligible decay (about 7.2%) after 10 h, which generally stayed ahead of commercial Pt/C catalysts (Figure 3(B)). The intrinsic superior ORR activity is also revealed by theoretical calculations (Figure 3(C)).

In addition, transition metal carbides have received significant attention owing to their eligible electronic structure around the Fermi level, which results in the outstanding activity and stability. However, agglomeration and structural collapse of nanoparticles usually occur during the formation of carbides. To this end, Yang et al.[45] embedded CoC_x into the *in-situ* grown carbon nanotubes (C@CoC_x) by a solid-solid separation method. The space-confinement effect of carbon nanotubes can effectively prevent the agglomeration of CoC_x nanoparticles. The crucial role of CoC_x in determining ORR activity was confirmed by showing higher ORR activity than the C@Co counterpart. In order to further improve the conductivity and accelerate the electron transfer, Jia et al.[46] coupled Fe_3C nanocrystalline with reduced graphene oxide (rGO), which displayed half-wave potential ($E_{1/2}$) of 0.8 V in 0.1 mol·L^{-1} KOH solution.

Featured with suitable changes in the d-band electronic structure, transition metal nitrides possess ex cellent electronic conductivity and improved ORR activity relative to their metal counterparts[49]. By a facile NH_3- histidine assisted project, Mu' group[47] fabricated unique Fe_xN nanoparticles implanted in N-doped carbon without Fe-N_4 motifs to clarify the important role of Fe_xN in ORR. Two main sites existed on the surface of Fe_2N, i.e., ε-Fe_2N and ζ-Fe_2N, with the former exhibiting superior catalytic activity demonstrated by DFT calculations. In ad dition, the activity of

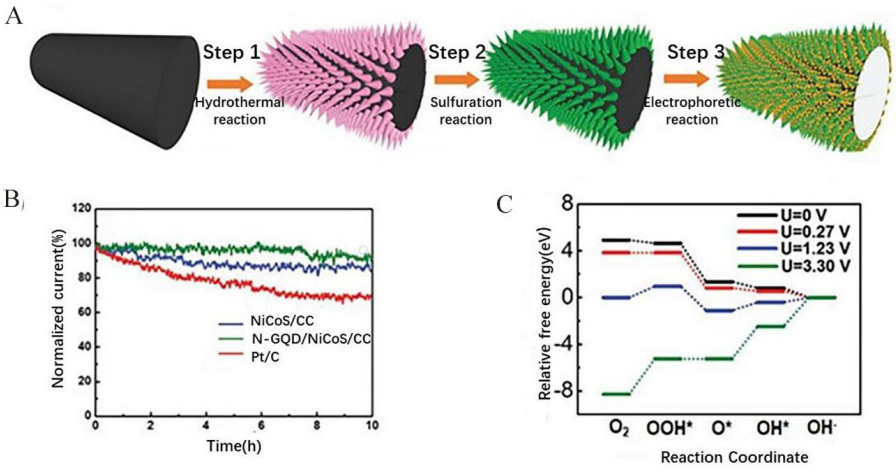

Figure 3 (A) Flow diagram for the synthesis processes of 3D N-GQDs/$NiCo_2S_4$/CC composite; (B) Durability testing curves in 0.1 mol·L^{-1} KOH; (C) Relative Gibbs free energy diagram of $NiCo_2S_4$ for the ORR at different potentials. Reproduced with permission of Ref. 54, copyright 2019 Wiley-VCH Verlag GmbH & Co. KGaA, Weinheim. (color on line)

the catalyst dropped significantly after removing Fe_xC with acid leaching (approximately 155 mV), further confirming the crucial role of Fe_xC as ORR site. Beyond single-metal nitrides, multi-metal nitrides have also been widely studied due to the tailored electronic structure by the secondary metals. Through solvothermal and nitriding treatment, Xia and Liao et al.[48] prepared $Ti_{0.8}Co_{0.2}N$ nanosheets with porous architectures, which demonstrated the improved ORR activity than Ti_xN. The $E_{1/2}$ of $Ti_{0.8}Co_{0.2}N$ was 0.85 V in an alkaline electrolyte, comparable to that of commercial Pt/C.

2.3 Transition-Metal Encapsulated in Graphitic Layers

In general, the bared transition metal-based nanocrystals in strong alkaline electrolytes are easily reconstructed or subject to Ostwald ripening, which in turn leads to the activity degradation. Recently, the concept about encapsulating nanoparticles of transition-metal and their derivatives in carbon shells has been proposed as an effective approach to protect the innermost components, yielding a new catalyst family, transition-metal encapsulated in graphitic layers[16]. Besides, a unique host-guest electronic interaction between metal nanoparticles and graphitic surface could activate the surface carbon shells and thus improving the ORR activity[55-58]. Inspired by the first discovery of Fe nanoparticles encapsulated in carbon nanotubes as active ORR catalyst[16], the ORR community has devoted intensive efforts to explore robust and stable catalysts structured in transition-metal encapsulated in graphitic layers, where the catalytic performance is greatly affected by the type of metal cores, thickness of carbon shell, and dopants into the carbon lattice.

Among the various candidates, Fe_3C encapsulated in graphitic layers or N-doped carbon nanotubes (Fe_3C@NG or Fe_3C@N-CNTs) has drawn immense attention due to Pt-like electronic structure[59-61]. Our group cooperated with Li's group[62] to develop a high-

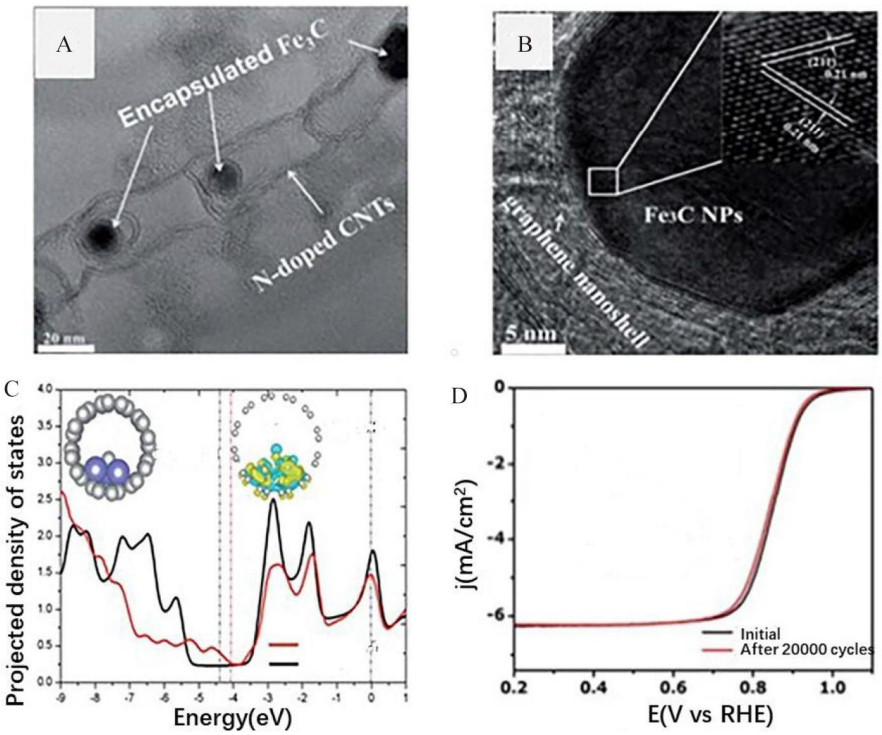

Figure 4 (A, B) Transmission electron microscopic images of Fe_3C encapsulated in N-doped carbon nanotubes/carbon black composite; (C) Results of the DFT calculations. PDOS of the p orbitals of C atoms bonded to Fe in Fe_3C@SWNT compared with that in pure SWNT; (D) ORR polarization plots after 20000 cycles in O_2-saturated 0.1 mol·L^{-1} KOH. Reproduced with permission of Ref. 63, copyright 2015 Royal Society of Chemistry. (color on line)

pressure pyrolysis strategy for the synthesis of hollow spheres of Fe_3C encapsulated in graphitic layers (Fe_3C/C). The uniform structure and the insignificant amount of N or Fe on the surface endow the catalyst as a distinctive model catalyst to identify the real active sites. Furthermore, a destructive test of the Fe_3C/C catalyst was conducted by ball-milling to destroy the protective carbon shells around the carbide nanoparticles and subject to acid leaching to remove the exposed Fe_3C nanoparticles. As a result, series activity decay was observed, suggesting the indispensable role of the Fe_3C core although it does not contact with the electrolyte directly. Later on, our group [63] encapsulated Fe_3C nanoparticles in bamboo-like N-doped carbon nanotubes/C through functionalizing the carbon substrate with oxygen containing species (Figure 4(A) and (B)). The strong electronic penetration effect from Fe_3C nanoparticles to the surface carbon is demonstrated to increase charge density near the Fermi level of C atoms and therefore reduce their local work function (Figure 4(C)). Owing to the electronic modification, the as-prepared catalyst showcases the excellent ORR activity and stability in 0.1 mol·L^{-1} KOH, with the mass activity of 8.27 A·g^{-1} at 0.9 V and only 6 mV shift in $E_{1/2}$ after 20000 cycles (Figure 4(D)). Further performance enhancement is achieved by constructing a meso/macroporous architecture via a simple pyrolysis method[64], which will be discussed in Section 3.1. In addition to Fe_3C, transition metal alloys are also explored as ideal core to construct the metal alloy encapsulated in graphitic layer catalyst. For example, CoFe[65-67], CoNi[68,69], FeNi[70,71] were reported to deliver higher activity than their corresponding individual components.

As mentioned above, dopants into the graphitic layer play an important role in the catalytic properties. On this basis, multi-heteroatoms doped carbons are developed as the shell for the transition metal encapsulation. For instance, P-doping can provide plentiful edge-defect sites and produce P^+ sites as extra active sites to further improve the ORR activity of carbon layers. Wang et al. [72] prepared the hollow spheres with CoFe alloyed nanoparticles encapsulated in N, P co-doped carbon nanovesicles using Vitamin B_{12} as Co and P resources. Due to the co-promotion effect of CoFe alloy and extra P doping, the charge density of the carbon atom adjected to N and P is significantly increased, such that boosting the oxygen electrocatalysis. Similarly, the S-doping can create defect sites to increase the active site density. By in-situ reducing Co_9S_8 through a two-step calcination method, novel electrocatalysts of cobalt nanoparticles embedded in N, S co-doped carbon matrix were prepared successfully. Specifically, the CoS-containing precursor was subject to the heat treatment at 800 °C under N_2 atmosphere to obtain CoS-1-800. In order to increase the N content of the catalyst, CoS-1-800 was mixed with an appropriate amount of melamine for secondary calcination to obtain CoSMe-X-800. The resultant catalyst possessed the onset potential and $E_{1/2}$ of 0.95 V and 0.85 V, respectively[73].

2.4 Atomically Dispersed Metal-Nitrogen-Carbon Materials

Downsizing the particle size to single atom affords the ultimate metal atom utilization and distinct electronic states of metal centers due to the discontinuous energy level distribution, and thereby tailoring the catalytic activity and selectivity. This concept was explicitly put forward by Qiao et al. in 2011[74], yet the pyrolyzed metal-nitrogen-carbon (M-N-C) materials with atomically dispersed M-N_x sites had been extensively studied for a long term, without being specifically named. And the atomic M-N_x sites were believed to be located inside the micropore of the carbon substrate[75]. On this basis, microporous metal organic frameworks (MOFs), especially zeolitic imidazolate frameworks (ZIFs) with carbon and nitrogen ligands, have been widely explored as the active site host. Using ZIF-8 as an active host, $Fe(acac)_3$ that provides Fe source was separately encapsulated into the cage of ZIF-8 due to the similar size between Fe $(acac)_3$ molecular and ZIF-8 cavity (Figure 5(A)). A thermal-treatment under an inert atmosphere transformed the precursor into the atomically dispersed Fe-N-C materials without Fe nanoparticles[76-78]. Apart from the ZIFs-confinement strategy, polymers-assisted

pyrolysis methods are also employed to prepare the atomically dispersed Fe-N-C catalysts. For instance, pyrrole-coated Fe_2O_3 nanorods[79], poly-p-phenylenediamine[80], and poly-1,8-diaminonaphthalene[81], that feature with rich nitrogen dopants and porosity, are developed for the preparation of Fe-N-C catalysts. In addition to the MOFs or polymers-assisted strategy, incorporating secondary atoms like Zn, Na, K, or Mg acting as the fences for avoiding the target metal atoms from intimate contacts is demonstrated effective to harvest atomically dispersed Fe-N-C catalysts[82-85]. Together with the preparation strategy booming, the activity of Fe-N-C catalyst has been improved to a Pt-like level. More excitingly, the active site structure can be elusively identified with the aid of atomic resolution STEM, Mössbauer spectroscopy and X-ray absorption spectroscopy (XAS). Taking our recent study for example[81], Fe-N-C derived from poly-1,8-diaminonaphthalene exhibits superior ORR activity to the state-of-the-art Pt/C. The microenvironment of the active sites was checked by aberration corrected STEM and XAS (Figure 5(B) and (C)), confirming atomically dispersed Fe coordinated with four nitrogen atoms as operational active sites.

Although Fe-N-C catalysts are considered as the most active M-N-C catalysts for ORR, they always suffer from Fenton reaction to generate poisoning reactive oxygen species, which will cause degradation of the catalysts and organic ionomers within electrodes. To mitigate Fenton effect, Lin' group[86] incorporated MnO_x into Fe-N-C catalyst, in which MnO_x can accelerate the decomposition of harmful H_2O_2, thus weakening the Fenton reactions. In addition to the above method, Co-N-C catalysts with mitigated Fenton reactions have been explored as a promising replacement for Fe-N-C catalysts. Similar to the case of Fe-N-C, ZIFs have attracted tremendous attention as precursors for Co-N-C, especially that the Co-based ZIF-67 and ZIF-8 are isomorphic, part of the Co atoms can be replaced by Zn atoms without changing the crystal structure. During the annealing treatment of ZnCo-ZIFs with controllable Zn/Co ratios, Zn^{2+} ions

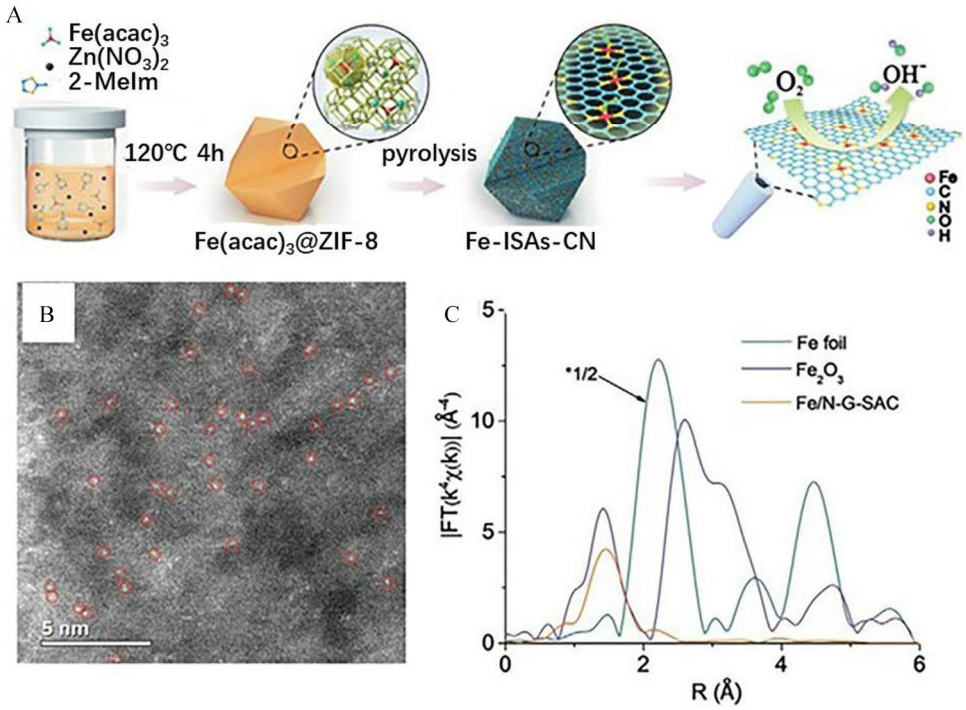

Figure 5 (A) Schematic illustration for the formation of Fe-N-C catalysts using ZIF-8 as an active site host; (B) Aberration-corrected HAADF-STEM image of the isolated Fe atoms involved Fe/N-G-SAC catalyst; (C) Fourier transforms of k^3-weighted Fe K-edge EXAFS data. Reproduced with permission of Ref. 81, copyright 2020 Wiley-VCH Verlag GmbH & Co. KGaA, Weinheim. (color on line)

can serve as a "fence" to further expand the adjacent distances of Co^{2+} ions, while Zn atoms are finally evaporated due to the low boiling point (e.g., 907 °C), such that Co-N-C catalysts with isolated Co atoms coordinated with nitrogen atoms are eventually obtained[59]. Other strategies, i.e., electrostatic spinning[87], polymer-assisted pyrolysis[88], are also developed. In spite of considerable progress achieved, the ORR activity of Co-N_x is intrinsically lower than that of Fe-N_x attributable to the weaker binding of O_2 on the Co center. Other metal centers, Mn[89], Zn[90], Ni[91] and Cu[92] are discovered as promising alternatives. For example, the outstanding ORR activity with $E_{1/2}$ of 0.9V was achieved on Mn-N-C[89]. Further efforts are required to push the activity of the iron-free M-M-C to a satisfactory level.

3 Structural Regulation

3.1 Hierarchically Porous Regulation

Engineering hierarchically porous nanostructures are extensively studied to modify the catalytic activity and stability of the heterogenous electrocatalysts due to the generated inherent advantages, i.e., large specific surface area towards increased density of surface active sites, accelerated reactants/products transportation, and enhanced accessibility of the active sites[93]. Therefore, proper tune on the pore structure could regulate the intrinsic activity and mass activity for ORR simultaneously.

As the micropore is regarded as the ideal host for active site deposition, yet it suffers from transfer resistance, hierarchically micro/mesoporous structure is favorable for enriching active site density and efficient mass transport. For example, 1D ion/nitrogen-doped carbon nanorods (Fe/N-CNRs) with a hierarchically micro/mesoporous structure were developed by Chen and co-workers[79] using 1D Fe_2O_3 nanorods derived from Fe-MIL-88B as both template and iron source (Figure 6(A)). The Fe_2O_3 nanorods could serve as an inducer to initiate pyrrole polymerization as it would be partially dissolved to generate Fe^{3+}. Consequently, the *in-situ* polymerized pyrrole would act as carbon, and nitrogen precursor. The unique pore structure guarantees an ultrahigh Brunauer-Emmett-Teller (BET) surface area of 666.7 $m^2 \cdot g^{-1}$ and a total pore volume of 1.3 $cm^3 \cdot g^{-1}$ (Figure 6(B) and (C)). Due to the merits, the as-obtained catalyst performs

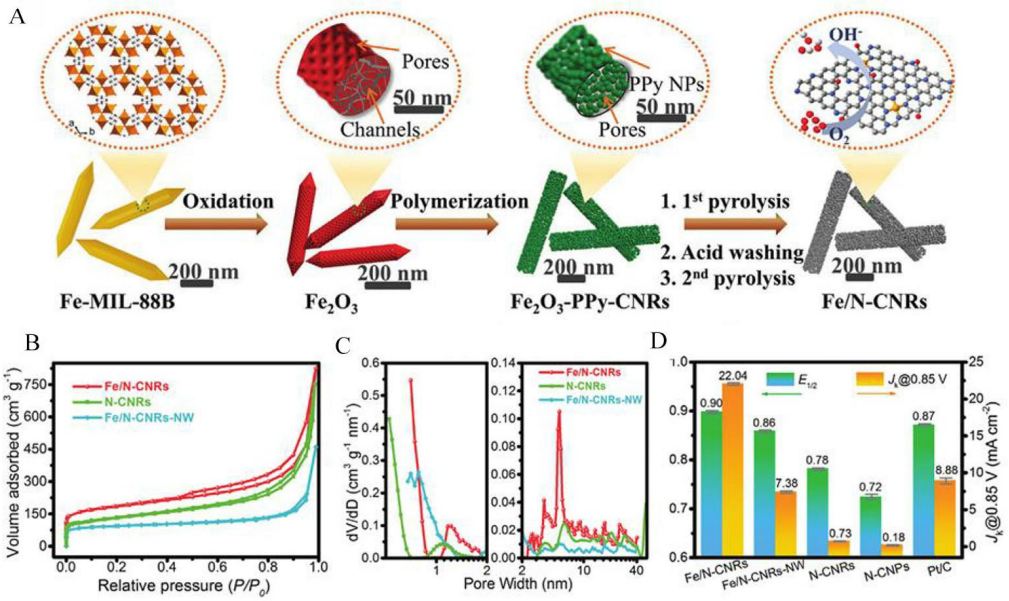

Figure 6 (A) Graphical illustration for the synthesis process of Fe/N-CNRs; (B) N_2 adsorption-desorption results and (C) Pore diameter distribution results for Fe/N-CNRs, N-CNRs, and Fe/N-CNRs-NW; (D) $E_{1/2}$ and kinetic current density (J_k)@0.85V results of these catalysts. Reproduced with permission of Ref. 79, copyright 2021 Wiley-VCH Verlag GmbH & Co. KGaA, Weinheim. (color on line)

outstanding ORR activity with the $E_{1/2}$ of 0.9 V, superior to that of Pt/C (Figure 6(D)). Combining the microporous Co-ZIFs with mesoporous FeNi-MIL, Chen's group cooperated with Wang's team[40] to prepare multimetal based porous nanorod catalyst with hierarchically micro/mesoporous structure (FeNiCo@NC-P) by the dual MOFs pyrolysis strategy. When employed as the air electrode in Zn-air batteries, the resultant micro/mesoporous FeNiCo@NC-P displays a low voltage gap of 0.84 V, much lower than that of the noble metal benchmarks (1.17 V).

Compared with the micropores or mesopores, macropores are more advantageous in promoting the mass transportation and thus decreasing the mass transfer polarization towards boosted reaction kinetics. Inspired by this, our group[64] engineered meso/macroporous nitrogen-doped carbon architectures consisting of iron carbide encapsulated in graphitic layers (Fe_3C/NG) through pyrolysis of poly(1,8-diaminonapphthalene) (PDAN) and a subsequent acid leaching procedure. The *in-situ* reduced Fe nanoparticles not only catalyze the graphitic carbon growth, but also serves as the hard template to form macropores. The multiple pore structure including both mesoporous and macroporous pores can be clearly observed from the N_2 adsorption-desorption curves. And the structural benefits are certified by showing excellent catalytic performance for ORR. Using polystyrene nanoparticle orderly assembled matrix as a template, the honeycomb-like Co-N_x-C catalyst with micro/macroporous structure was fabricated by Chen and co-workers[94]. Owing to the interconnected ordered macropores throughout the electrocatalyst, active sites are able to smoothly "exhale/inhale" reactants and products, enhancing the accessibility of active sites and the reaction kinetics when applied as an air electrode in the Zn-air batteries. Later on, they utilized silica nanoparticles as hard templates for the preparation of meso/macroporous carbon spheres with densely anchored Fe-N_x sites (SA-Fe-N_x-MPCS), as shown in Figure 7(A)[80]. Compared with bulk solid carbon-based catalyst (SA-FE-N_x-SC) electrode, the hierarchically porous framework of SA-Fe-N_x-MPCS delivers uncomplicated access of the oxygen to active

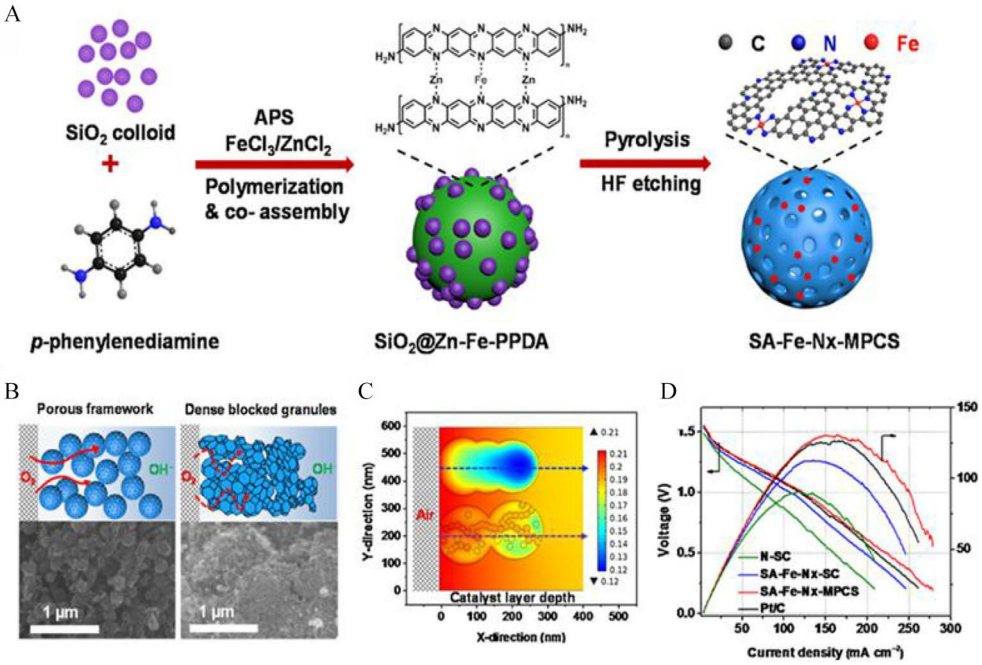

Figure 7 (A) Synthetic scheme for the preparation of SA-Fe-N_x-MPCS catalyst; (B) Schematic illustration of the air electrodes and their SEM images; (C) COMSOL multiphysics modeling of O_2 diffusion into the air electrode; (D) Polarization and power density curves of flow batteries with the prepared catalysts and Pt/C. Reproduced with permission of Ref. 80, copyright 2021 Elsevier. (color on line)

sites and thus affording rich available triple-phase reaction zone for ORR (Figure 7(B)). The reaction-diffusion model constructed by COMSOL multiphysics shows that MPCS exhibit less gaseous oxygen transfer resistance and the solid granules are beneficial to construct the pathways for the diffusion of O_2, thus boosting cell performance (Figure 7(C)). As a result, the as-designed catalyst results in exceptional performance with a large peak power density of 130 mW·cm^{-2} (Figure 7(D)).

3.2 Interface Engineering

For the heterogenous catalysts, their catalytic performance is highly subject to the surface/interface properties of the catalyst, which not only determines the adsorption strength toward the intermediates, but also affects the charge and mass transfer behaviors. Bearing this in mind, proper tune on interface structure of heterogenous catalysts is regarded as a promising approach to boost the intrinsic electrocatalytic activity. For instance, chemical coupling of CoO nanoclusters and Mn_3O_4 nano-octahedrons to engineer high-energy interfacial structures leads to a notable enhancement on ORR activity compared with either CoO or Mn_3O_4[95]. Nonetheless, the semi-conductivity of metal oxides impedes the catalysts from unleashing their intrinsic activity completely. To address the electronic conductivity issue, the defective carbon-CoP interfacial structure was constructed and it exhibited outstanding bifunctional activity, benefiting from interfacial charge polarization[96]. However, the long-term stability of defective carbon was questionable in the harsh electrochemical condition. Further optimization of interfacial structure to improve intrinsic activity, electronic conductivity, and stability simultaneously is highly requirable.

To this regard, our group[70] engineered the metal-

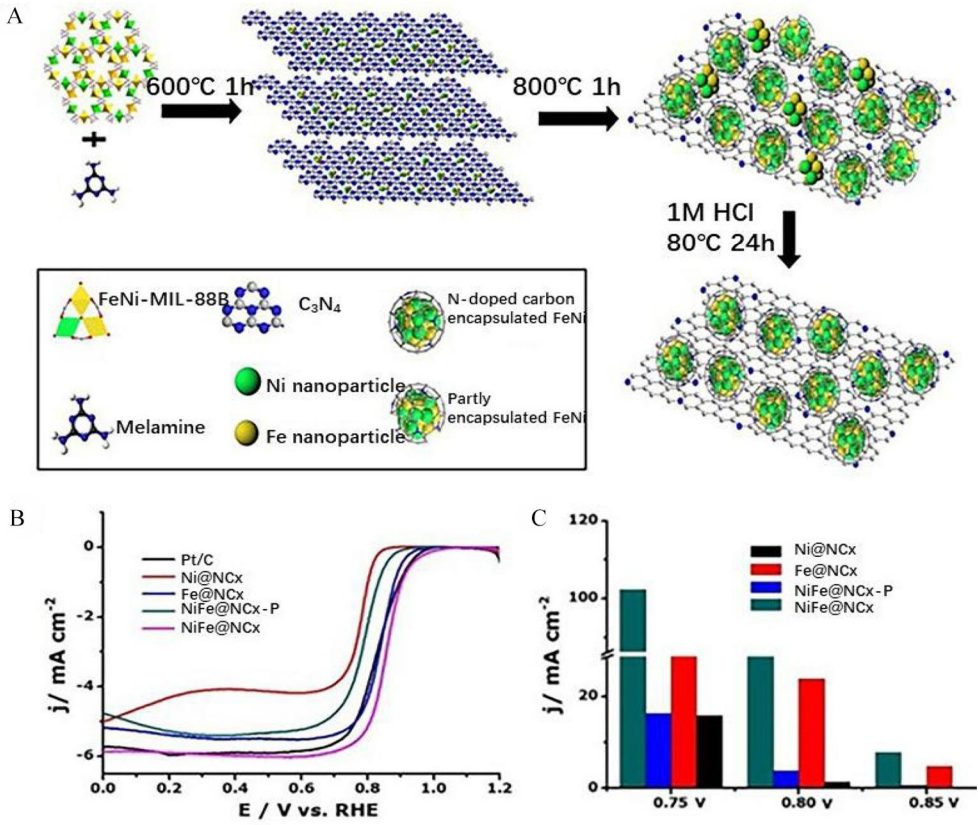

Figure 8 (A) Schematic illustration revealing the synthetic strategy of the TMs@NC$_x$ composite; (B) ORR polarization curves for TMs@NC$_x$ samples in O_2-saturated 0.1 mol·L^{-1} KOH at scan rate of 5 mV·s^{-1} and rotation speed of 1600 r·min^{-1}; (C) J_k of ORR at different potentials on different catalysts. Reproduced with permission of Ref. 70, copyright 2016 American Chemical Society. (color on line)

carbon interfacial structure employing metal-organic-frameworks (MOFs)-assisted two-stage encapsulation strategy (Figure 8(A)). The metallic alloy core and highly graphitic carbon shell guarantee the excellent electronic conductivity. Through precisely tuning the metal core, the electronic penetration effect from metal core to carbon shell could be well regulated and thus leading to significantly enhanced ORR activity. In his study, different transition metal cores, i.e., Ni, Fe and NiFe alloy, were selected as metal cores, and the resultant catalysts are denoted as Ni@NC_x, Fe@NC_x, and NiFe@NC_x, respectively. As shown in Figure 8(B), NiFe@NC_x displayed much higher $E_{1/2}$ (0.86 V) than Ni@NC_x (0.78 V) and Fe@NC_x (0.84 V). Moreover, it also delivered higher kinetic current density at the fixed potentials than the Ni@NC_x and Fe@NC_x counterparts (Figure 8(C)). The excellent catalytic activity of NiFe@NC_x enabled superior gravimetric energy density of 732.3 Wh·kg_{Zn}^{-1}, against that of the Pt/C+IrO_2-based battery (the energy density of 543.2 Wh·kg_{Zn}^{-1}). To further increase the catalytic activity, we constructed an exquisite triphasic interfacial structure consisting of encapsulated Fe_xNi alloy, graphitic shell and a partially exposed FeO_y thin-layered surface[97]. This design was accomplished by the incorporation of Ni, which can adjust the oxidation degree of surface Fe as well as the electronic structure of the *in-situ* formed Fe oxide (Figure 9(A)). The HRTEM image clearly demonstrates the crucial role of Ni in determining the thickness and electronic states of the surface FeO_y phase (Figure 9(B)). At an optimal Ni content, the thin-layer FeO_y phase not only participates in constructing active interfacial structure, but also accelerates electron conduction to guarantee the excellent electronic conductivity of oxide-involved structure. Therefore, the hybrid catalyst outperforms the commercial noble-metal benchmarks with a higher $E_{1/2}$ of 0.890 V for ORR.

To fulfill good bifunctionality of oxygen electrocatalysis, engineering metal phosphides-based hetero-

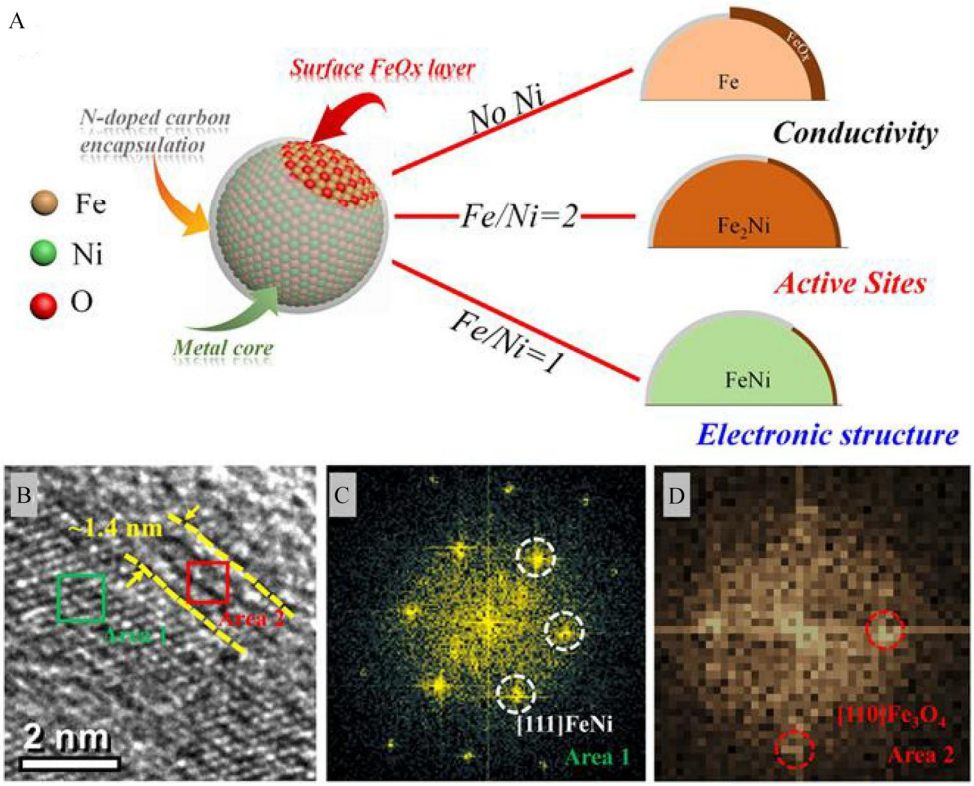

Figure 9 (A) Schematic illustration for the Ni doping strategy to regulate the interface structure of the as-derived catalysts; (B) RTEM image, and (C, D) FFT patterns derived from the regions of the areas 1 and 2 in (B). Reproduced with permission of Ref. 97, copyright 2020 Wiley-VCH Verlag GmbH & Co. KGaA, Weinheim. (color on line)

inter face structure represents a promising approach as metal phosphides are hailed as one of the most effective OER electrocatalysts. Chen's group[98] reported the CoO/Co_xP heterostructured nanoparticles anchored on N-rich nanosheets by a facile, one-step phosphorization process of layered cobalt (II) hexamethylenetetramine MOFs. The cooperation between these components was unveiled by theoretical calculations, which showing a moderate adsorption energy of OOH on CoO (111) surface (-1.03 eV) and relatively low O_2 binding energy on CoP (211) surface (0.02 eV). As a result, CoO and Co_xP mainly contribute to ORR and OER in the hybrid, respectively. The electrocatalytic measurements further confirm the superiority of this heterointerface structure design by showing $E_{1/2}$ of 0.86 V for ORR and overpotential of 370 mV at 10 mA·cm^{-2} for OER. Later on, an improvement was achieved by engineering multi-components-based interface structure with a well-designed Fe_2Ni_MIL-88@ZnCo_ZIF composite as precursors[40]. The derived catalyst featured with CNT-grafted, N-doped carbon nanorod embedded with Fe-Ni-Co metal/metal phosphide nanoparticles (denoted as FeNiCo@NC-P). Its outstanding bifunc tional oxygen electrocatalytic performance was evidenced by exhibiting a low charge-discharge voltage gap and an impressive long-term stability over 130 h when serving as an air electrode for rechargeable Zn-air battery protype.

In addition to the different active phase surface/interface interactions, the metal-support interaction is also vital for performance improvement due to its ability in tuning the electronic structures of the supported metals. Carbon-based materials are widely explored as ideal supports due to the excellent conductivity and strong interaction with the supported metals. For example, Hou et al.[99] anchored Fe_xN nanoparticles on N-doped graphene oxide surface through assistance of π-π stacking between iron phthalocyanine and oxygen containing functional groups in GO, thus providing an electronic transmission channel and preventing the agglomeration of Fe_xN in pyrolysis process. Electrochemical tests show that the ORR performance of hybrid was significantly better than those of pure GO, single Fe_xN and their mechanical mixtures, implying a strong interaction occurred between Fe_xN and GO. Coincidentally, Liao et al.[100] prepared the $TiCoN_x$ nitride nanoparticles on N-doped reduced graphene oxide (rGO), yielded $E_{1/2}$ of 0.902 V better than that of commercial Pt/C approaching to 30 mV.

3.3 Defect Engineering

Defect engineering provides a feasible and efficient approach to tailor the catalytic performance of the electrocatalysts as the introduction of defects is proven to regulate the electronic and surface properties of catalysts towards enhanced intrinsic activity. For the metal-free carbon materials, the electronic state could be asymmetrically tailored at the vacancy or reconstructed carbon defect sites, resulting in enhanced ORR activity in comparison to the pristine carbon with perfect hexagonal lattice. Taking advantages of both defect and dopants, our group[31] strategically engineered edge defects with selectively doped pyridinic N and pyrrolic N by an *in-situ* released CO_2 activation method with nano-$CaCO_3$ as the template. The total portion of pyridinic N and pyrrolic N reached up to 94% in the as-derived catalyst, which enables high $E_{1/2}$ of 0.853 V, and comparable Tafel slope of 58 mV·dec^{-1} to that of the commercial Pt/C benchmark (62 mV·dec^{-1}).

The defect in carbons not only can tailor the electronic structure of carbon atoms to activate the inert carbons, but also generate strong metal-support interaction in the carbon-metal compound hybrids for synergetic oxygen electrocatalysis. Take the work of Chen's group for example[43], the defect-enriched N-doped graphene quantum dots (GQDs) were intentionally engineered with 3D $NiCo_2S_4$ nanoarray as an active and a stable air cathode for rechargeable Zn-air battery. The synergistic effect between N-GQDs and $NiCo_2S_4$ facilitate the adsorption of OOH* and desorption of OH*, thus leading to faster ORR kinetics. Besides, the strong coupling and synergetic interaction between N-GQDs and $NiCo_2S_4$ nanoarray ensure the long-term durability and high flexibility of the home-made Zn-air battery device.

More interestingly, our recent study[81] reveals that engineering carbon defect to expose active FeN_4 edge sites could significantly improve the catalytic activity of atomically dispersed Fe-N-C. As well known, the local carbon structure surrounding FeN_4 moiety plays a key role in determining the final catalytic properties, with FeN_4 located at the edge superior to the one in plane. Bearing this in mind, we aimed at engineering FeN_4 edge sites embed onto the defective carbon matrix using a self-sacrificed Fe templating approach, the catalyst was denoted as Fe/N-G-SAC. This strategy was firstly rationalized by DFT calculations, demonstrating that the atomic FeN_4 moieties are preferentially deposited onto the nearby Fe clusters and the removal of Fe clusters would lead to the edge site exposure (Figure 10(A-D)). The reduced coordination number of edge N (N-C coordination number of 1) against the in-plane sites (N-C coordination number of 2) causes the increased electron transfer from Fe to the adjacent N atom in the former, and thereby, the negative shift of the d-band center on the edge of FeN_4 site. Consequently, the weakened OH adsorption energy was observed on the edge site, corresponding to a faster OH desorption process, which is generally considered as the rate-determining step on the atomic Fe site (Figure 10(E)). The concept-of-proof study confirmed the structure advantage of Fe/N-G-SAC over other samples. As shown in Figure 10(F), it displayed the most positive $E_{1/2}$ of 0.89 V, even better than the commercial Pt/C-JM catalyst.

3.4 Atomic Pair Construction

Typically, the well-defined active site M-N_x-C_y in the atomically dispersed M-N-C catalysts is formed by single transition metal atoms coordinated with four atoms in the same plane (N or C atoms in most cases). The catalytic performance is directly determined by the structure of M-N_x-C_y, i.e., coordination number, bond length and local carbon environment. On this basis, the atomic-scale regulation on the M-N_x-C_y structure would generate huge influence on the catalytic performance. The incorporation of secondary metal atoms into the M-N-C catalysts to generate a so-called atomic pair site, was found to be more effectively to boost catalytic activity very recently. For instance, using bi/tri-metallic zeolitic imidazolate frameworks (ZIFs) with controllable metal ratio,

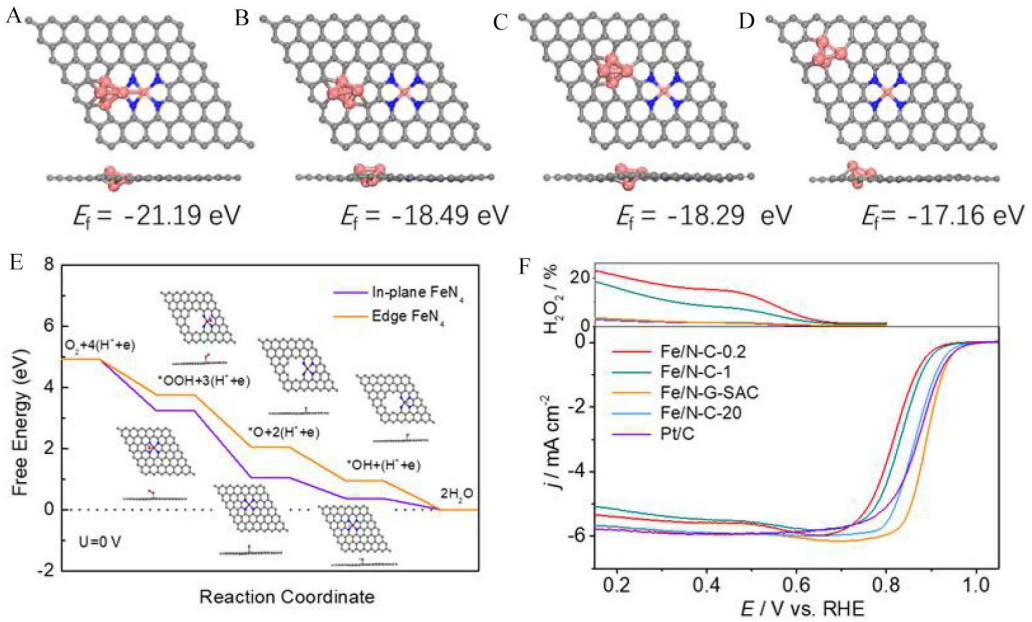

Figure 10 (A-D) Various Fe cluster/Fe-N_4 site configurations and the corresponding formation energy (E_f); (E) ORR Gibbs free energy diagrams on the edge and in-plane sites; (F) ORR polarization curves of the Fe/N-G-SAC, other Fe-based counterparts and the commercial Pt/C. Reproduced with permission of Ref. 81, copyright 2020 Wiley-VCH Verlag GmbH & Co. KGaA, Weinheim. (color on line)

our group successfully developed the Co_2N_5[101] and $FeCoN_5$[102] atomic pair site. And the superiority of the atomic pair site to the single-atom counterparts was confirmed by showing more than one magnitude higher activity than single-atom counterparts. Both the geometric structure advantage and OH-ligand self-binding modulation effect are proposed to be responsible for the enhanced activity.

Employing a similar ZIFs-assisted host-guest strategy (Figure 11(A)), a novel asymmetric $IrCoN_5$ atomic pair structure was exquisitely deigned towards enhanced Co-O affinity[103]. Since the chemical adsorption of oxygen on Co site involves the overlapping of oxygen orbital with the partially occupied Co d_{z2} orbital and d_{yz} orbital, the atomic Ir incorporation would break the electronic configuration symmetry of pristine Co 3d-orbital and thus inducing electron rearrangement with lower occupancy of d_{z2} orbital for strengthened oxygen adsorption. The hypothesis was validated by computing partially density of states

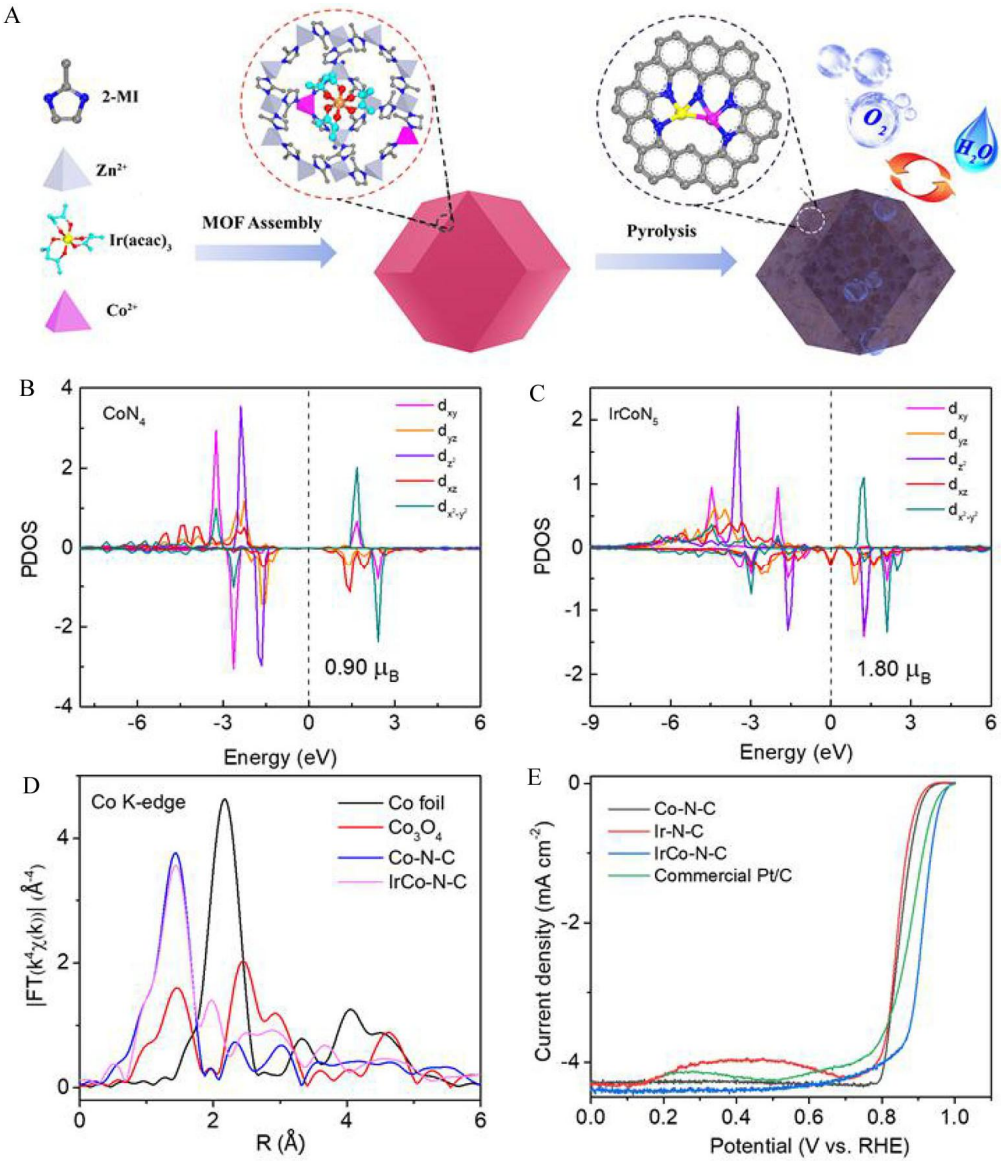

Figure 11 (A) Schematic illustration for the synthetic procedure of diatomic IrCo-N-C catalyst; (B, C) Partial density of states for Co-3d orbitals in (B) CoN_4, (C) $IrCoN_5$; (D) Fourier transformed extended X-ray adsorption fine structure (FT-EXAFS) spectra at Co K-edge; (E) The ORR polarization curves of IrCo-N-C, single-atom Co-N-C and Ir-N-C, and commercial Pt/C in 0.1 mol·L^{-1} KOH solution. Reproduced with permission of Ref. 103, copyright 2021 American Chemical Society. (color on line)

(PDOS) of Co, which shows a larger spin magnetic moment (1.80 μB vs. 0.90 μB) on the Ir-Co atomic pair site (Figure 11(B) and (C)). And the strengthened Co-O affinity was confirmed by Crystal Orbital Hamilton Population (COHP) analysis. The atomic pair structure was systematically examined by aberration corrected high-angle annular dark-field scanning transmission electron microscopy (HAADF-STEM) and X-ray absorption fine structure (XAFS) spectroscopy, confirming the presence of Ir-Co bond with the distance of about 2.30 Å and Ir-N coordination number of 3 (Figure 11(D)). Combined with the theoretical calculations, the active site structure is elucidated as $IrCoN_5$. Due to the structural merits, the catalyst containing atomic pair site exhibited superior ORR activity to the single-atom Co-N-C and Ir-N-C counterparts by showing a more positive $E_{1/2}$ of 0.911 V (0.85 V for Co-N-C; 0.845 V for Ir-N-C; Figure 11(E)). Such an electrocatalytic activity improvement is further verified by the excellent power density and cyclability in a homemade rechargeable Zn-air battery.

Apart from the short-range metal-metal modulation, metal-N_x could impose electronic effect on the adjacent metal-N_x moiety through long-range interaction. A very recent work reported by Jin et al.[104] also highlighted the importance of inter-site distance effect in the Fe-N-C SACs. They claimed that the increased intrinsic ORR activity was resulted from strong interactions between adjacent Fe-N_4 moieties altering the electronic structure when the inter-site distance is less than about 1.2 nm. On this basis, Chen and co-workers[105] employed atomic Fe-N_x species to regulate the coordination environment of single atom Ni site towards the regulated Ni/N-O coordination number. The well-designed FeNi atomic pair electrocatalyst (FeNi-SAs@NC) was prepared by simply pyrolyzing the mixture of metal salts, urea and carbon black. The atomic structure of the catalyst was carefully studied by aberration corrected HAADF-STEM and XAFS spectroscopy, revealing the atomic dispersion of Fe and Ni species. The Ni-N coordination numbers determined by the fitting analysis of Fourier transformed extended X-ray absorption fine structure (FT-EXAFS) were found to be 4.1 and 5.6 for Ni-SAs@NC and FeNi-SAs@NC, respectively, indicating that the introduction of isolated Fe moieties modulated the local coordination environment of adjacent Ni-SAs due to relatively lower electronegativity of Fe (1.83 vs. 1.91 for Ni). As a result, the inert Ni atoms can be activated through a more favorable oxygen adsorption process. Besides, the distorted Ni single atoms cooperate with Fe atoms and synergistically co-contribute to the ORR activity. These attributes endow the FeNi-SAs@NC with the higher ORR activity than both the Ni-SAs@NC and Fe-SAs@NC.

4 Conclusions and Perspectives

The development of cost-effective and high-performance ORR electrocatalysts to replace the expensive Pt-based materials faces one of the biggest challenges for the widespread employments of AEMFCs and metal-air batteries. The past decades have witnessed significant progress in terms of category diversity and performance enhancement. The advancements of four typical NPMCs including metal-free carbon-based materials, metal compounds, metal encapsulated in graphitic layer and atomically dispersed metal-nitrogen-carbon materials are summarized with the emphasis on their active site structure identification. And the properties of the materials involved in this review are compared in Table 2. Due to the heterogenous structure in most of these catalysts, it is hard to definitely claim the absolute active site structure. Commonly, more than one sites cooperatively contribute to the overall activity. Thanks to the appearance of the atomically dispersed metal-nitrogen-carbon (M-N-C) catalysts and the advanced characterization techniques, we could distinguish the predominated active site as the atomic M-N_x species own the highest intrinsic activity. With the knowledge on the typical NPMCs and the main active site structure of each category, the structural regulation strategies towards improved catalytic activity are emphatically discussed because the structure determines the active site accessibility, the intrinsic activity and the mass/electron transportation. It can be clearly found

that with a deeper understanding on the structure-activity relationship from a nanoscale to an atomic scale, the structure regulation strategies are switched from the pore structure engineering to the atomic active site manipulation.

In spite of the great achievement made in the structural regulation on the NPMCs for ORR in alkaline electrolytes, several challenges should be well tackled in future for their practical implementation in the fuel cells and batteries. Firstly, more effective synthetic strategies are highly desirable, especially for the atomically dispersed M-N-C materials. The current preparation approaches always limit the metal loading to less than 1wt%, corresponding to low site den-

Table 2 The ORR performance and synthesis method of the representative NPMCs reported in literature.

Sample	$E_{1/2}$(V vs. RHE)	Synthesis method
N-doping carbon[31]	0.853	Template method
N, S co-doping carbon[34]	0.83	Hummers' method
N, S, O tri-doped carbon nanosheet[37]	0.86	Template method
VACNTs-MnO_2[38]	/	Nebulized ethanol assisted infiltration and pyrolysis method
Mn@$LaCoO_3$[39]	0.72	Polyol-assisted solvothermal method
FeNiCo-P[40]	0.84	Pyrolysis method
Co_2P -Co, N, and P multi-doped carbon material[41]	0.843	Phosphidation
C@CoC_x[45]	0.8	Solid-solid separation method
Fe_3C@ rGO[46]	0.8	Pyrolysis method
Fe_xN@N-doped carbon[47]	0.84	NH_3- histidine assisted method
NiCo-P[52]	0.82	Electrospinning route
$NiCo_2S_4$@g-C_3N_4-CNT[53]	0.76	Two-step hydrothermal
N-GQDs@$NiCo_2S_4$[54]	0.86	Hydrothermal, sulfuration and electrophoretic deposition
Fe_3C/N-doped carbon[64]	0.86	Pyrolysis method
CoFe/N, P co-doped carbon nanovesicles[72]	086	Impregnation and pyrolysis method
Co/N, S co-doped carbon[73]	0.85	Two-step calcination methods
Pt_1/FeO_x[74]	/	Pyrolysis method
Fe/N-CNRs[79]	0.9	Pyrolysis method
SA-Fe-N_x-MPCS[80]	0.88	Template method
Fe/N-G-SAC[81]	0.89	Template method
Co-N_x-C[94]	/	Template method
CoO@Mn_3O_4[95]	/	Adsorption and reduction method
carbon-CoP[96]	0.81	Phosphorization method
Fe_xN[97]	0.89	Pyrolysis method
CoO/Co_xP[98]	0.86	Phosphorization method
Fe_xN@N-doped GO[99]	/	Pyrolysis method
$TiCoN_x$-rGO[100]	0.902	Pyrolysis method
Co_2N_5[101]	0.79	Pyrolysis method
$FeCoN_5$[102]	0.86	Pyrolysis method
$IrCoN_5$[103]	0.911	ZIFs-assisted host-guest method
FeNi-SAs@NC[105]	0.907	Pyrolysis method

sity. This will lead to thick catalyst layer upon transferring the catalyst into the gas diffusion electrode, in turn causing mass transport issues. Secondly, the structural stability, especially the dynamic stability should be taken into consideration. For instance, although the defective carbon is more active than well-graphitized ones, its stability under harsh electrochemical conditions is questionable. There might be a trade-off between the activity and stability. Similarly, for the interfacial structure, the tight contacts between the interface components need be well maintained via either covalent bond or electrostatic interaction. Not only the efficient preparation strategies, but also the operando characterization techniques are imperative to address the structure stability issues. Last but not the least, precise control of the atomic pair site structure and more comprehensive mechanistic insights into the synergy of the adjacent sites remain the biggest challenge to push forward the field. This calls for the delicate design of the precursor, advancement of atomic-scale resolution characterizations and combination of theoretical modeling under realistic working conditions. Despite the challenges still ahead, we optimistically believe that recent advances and continuing efforts will eventually realize the practical applications of NPMCs in the fuel cells and metal air batteries, and also inspire more advances in catalytic chemistry for other applications.

Acknowledgements:

The authors thank the National Key R&D Program of China (2018YFB1502400), the National Natural Science Foundation of China (21633008, U1601211, 21733004), the Strategic Priority Research Program of the Chinese Academy of Sciences (XDA21090400), the Department of Science and Technology of Shandong province (2019JZZY010905), and the Jilin Province Science and Technology Development Program (20190201300JC, 20170520150JH, 20200201001JC) for financial supports.

References:

[1] Lewis N S, Nocera D G. Powering the planet: Chemical challenges in solar energy utilization[J]. PNAS, 2006, 103 (43): 15729-15735.

[2] Arges C G, Ramani V, Pintauro P N. Anion exchange membrane fuel cells[J]. Electrochem. Soc. Interface, 2010, 19 (2): 31-35.

[3] Cheng F Y, Chen J. Metal-air batteries: from oxygen reduction electrochemistry to cathode catalysts[J]. Chem. Soc. Rev., 2012, 41(6): 2172-2192.

[4] Nörskov J K, Rossmeisl J, Logadottir A. Origin of the overpotential for oxygen reduction at a fuel-cell cathode [J]. J. Phys. Chem. B, 2004, 108(46): 17886-17892.

[5] Niu W J, He J Z, Gu B N, Liu M C, Chueh Y L. Opportunities and challenges in precise synthesis of transition metal single - atom supported by 2D materials as catalysts toward oxygen reduction reaction[J]. Adv. Funct. Mater., 2021, 31 (35): 2103558.

[6] Liu M M, Wang L L, Zhao K N, Shi S S, Shao Q S, Zhang L, Sun X L, Zhao Y F, Zhang J J. Atomically dispersed metal catalysts for the oxygen reduction reaction: synthesis, characterization, reaction mechanisms and electrochemical energy applications[J]. Energy & Environ Sci., 2019, 12(10): 2890-2923.

[7] Wu G, Zelenay P. Nanostructured nonprecious metal catalysts for oxygen reduction reaction[J]. Acc. Chem. Res., 2013, 46(8): 1878-1889.

[8] Feng Y, Alonso-Vante N. Nonprecious metal catalysts for the molecular oxygen-reduction reaction[J]. Phys. Status Solidi, 2010, 245(9): 1792-1806.

[9] Zhu C Z, He L, Fu S F, Dan D, Lin Y H. Highly efficient nonprecious metal catalysts towards oxygen reduction reaction based on three-dimensional porous carbon nanostructures[J]. Chem. Soc. Rev., 2016, 45(3): 517-531.

[10] Gong K P, Du F, Xia Z H, Durstock M, Dai L M. Nitrogen-doped carbon nanotube arrays with high electrocatalytic activity for oxygen reduction[J]. Science, 2009, 323(5915): 760-764.

[11] Zhang L P, Lin C Y, Zhang D T, Gong L L, Zhu Y H, Zhao Z H, Xu Q, Li H J, Xia Z H. Guiding principles for designing highly efficient metal-free carbon catalysts[J]. Adv. Mater., 2019, 31(13): 1805252.

[12] Daems N, Sheng X, Vankelecom I F J, Pescarmona P P. Metal-free doped carbon materials as electrocatalysts for the oxygen reduction reaction[J]. J. Mater. Chem. A, 2014, 2(12): 4085-4110.

[13] Quílez-Bermejo J, Morallón E, Cazorla-Amorós D. Metal-free heteroatom-doped carbon-based catalysts for ORR: A critical assessment about the role of heteroatoms [J]. Carbon, 2020, 165: 434-454.

[14] Liang Y Y, Li Y G, Wang H L, Zhou J G, Wang J, Regier T, Dai H J. Co_3O_4 nanocrystals on graphene as a synergistic catalyst for oxygen reduction reaction[J]. Nat. Mater., 2011, 10(10): 780-786.

[15] Odedairo T, Yan X C, Ma J, Jiao Y L, Yao X D, Du A J, Zhu Z H. Nanosheets Co_3O_4 interleaved with graphene for highly efficient oxygen reduction[J]. ACS Appl. Mater. Interfaces, 2015, 7(38): 21373-21380.

[16] Deng D H, Yu L, Chen X Q, Wang G X, Jin L, Pan X L, Deng J, Sun G Q, Bao X H. Iron encapsu lated within pod-like carbon nanotubes for oxygen reduction reaction [J]. Angew. Chem. Int. Ed., 2013, 52(1): 371-375.

[17] He Y H, Liu S W, Priest C, Shi Q R, Wu G. Atomically dispersed metal-nitrogen-carbon catalysts for fuel cells: advances in catalyst design, electrode performance, and durability improvement [J]. Chem. Soc. Rev., 2020, 49(11): 3484-3524.

[18] Chen M J, He Y H, Spendelow J S, Wu G. Atomically dispersed metal catalysts for oxygen reduction[J]. ACS Energy Lett., 2019, 4(7): 1619-1633.

[19] Zhu Y Z, Sokolowski J, Song X C, He Y H, Mei Y, Wu G. Engineering local coordination environments of atomically dispersed and heteroatom-coordinated single metal site electrocatalysts for clean energy-conversion[J]. Adv. Energy. Mater., 2020, 10(11): 1902844.

[20] Pan Y, Zhang C, Liu Z, Chen C, Li Y D. Structural regulation with atomic-level precision: from single-atomic site to diatomic and atomic interface catalysis[J]. Matter, 2020, 2(1): 78-110.

[21] Liu D B, He Q, Ding S Q, Song L. Structural regulation and support coupling effect of single-atom catalysts for heterogeneous catalysis[J]. Adv. Energy. Mater., 2020, 10 (32): 2001482.

[22] Ling T, Jaroniec M, Qiao S Z. Recent progress in engineering the atomic and electronic structure of electrocatalysts via cation exchange reactions[J]. Adv. Mater.,2020, 32(46): 2001866.

[23] Zhang L P, Xu Q, Niu J B, Xia Z H. Role of lattice defects in catalytic activities of graphene clusters for fuel cells[J]. Phys. Chem. Chem. Phys., 2015, 17(26): 16733-16743.

[24] Jia Y, Zhang L Z, Zhuang L Z, Liu H L, Yan X C, Wang X, Liu J D, Wang J C, Zheng Y R, Xiao Z H, Taran E, Chen J, Yang D J, Zhu Z H, Wang S Y, Dai L M, Yao X D. Identification of active sites for acidic oxygen reduction on carbon catalysts with and without nitrogen doping [J]. Nat. Catal., 2019, 2(8): 688-695.

[25] Hu C G, Paul R, Dai Q B, Dai L M. Carbon-based metal-free electrocatalysts: from oxygen reduction to multifunctional electrocatalysis[J]. Chem. Soc. Rev., 2021, 50(21): 11785-11843.

[26] Gao F, Zhao G L, Yang S, Spivey J J. Nitrogen-doped fullerene as a potential catalyst for hydrogen fuel cells[J]. J. Am. Chem. Soc., 2013, 135(9): 3315-3318.

[27] Sidik R A, Anderson A B, Subramanian N P, Kumaraguru S P, Popov B N. O_2 reduction on graphite and nitrogen-doped graphite: experiment and theory[J]. J. Phys. Chem. B, 2006, 110(4): 1787-1793.

[28] Xing T, Zheng Y, Li L H, Cowie B C C, Gunzelmann D, Qiao S Z, Huang S M, Chen Y. Observation of active sites for oxygen reduction reaction on nitrogen-doped multilayer graphene[J]. ACS Nano, 2014, 8(7): 6856-6862.

[29] Guo D H, Shibuya R, Akiba C, Saji S, Kondo T, Nakamura J. Active sites of nitrogen-doped carbon materials for oxygen reduction reaction clarified using model catalysts[J]. Science, 2016, 351(6271): 361-365.

[30] Ding W, Wei Z D, Chen S G, Qi X Q, Yang T, Hu J S, Wang D, Wan L-J, Alvi S F, Li L. Space-confinement-induced synthesis of pyridinic- and pyrrolic-nitrogen-doped graphene for the catalysis of oxygen reduction[J]. Angew. Chem. Int. Ed., 2013, 52(45): 11755-11759.

[31] Luo E G, Xiao M L, Ge J J, Liu C P, Xing W. Selectively doping pyridinic and pyrrolic nitrogen into a 3D porous carbon matrix through template-induced edge engineering: enhanced catalytic activity towards the oxygen reduction reaction[J]. J. Mater. Chem. A, 2017, 5(41): 21709-21714.

[32] Silva R, Al-Sharab J, Asefa T. Edge-plane-rich nitrogen-doped carbon nanoneedles and efficient metal-free electrocatalysts[J]. Angew. Chem. Int. Ed., 2012, 51(29): 7171-7175.

[33] Zhao Y, Yang L J, Chen S, Wang X Z, Ma Y W, Wu Q, Jiang Y F, Qian W J, Hu Z. Can boron and nitrogen co-doping improve oxygen reduction reaction activity of carbon nanotubes?[J]. J. Am. Chem. Soc., 2013, 135(4): 1201-1204.

[34] Zhu J B, Li K, Xiao M L, Liu C P, Wu Z J, Ge J J, Xing W. Significantly enhanced oxygen reduction reaction performance of N-doped carbon by heterogeneous sulfur incorporation: synergistic effect between the two dopants in metal-free catalysts[J]. J. Mater. Chem. A, 2016, 4(19): 7422-7429.

[35] Chen W, Chen X, Qiao R, Jiang Z, Jiang Z J, Papovi? S, Raleva K, Zhou D. Understanding the role of nitrogen and sulfur doping in promoting kinetics of oxygen reduction reaction and sodium ion battery performance of hol-

low spherical graphene[J]. Carbon, 2022, 187: 230-240.

[36] Razmjooei F, Singh K P, Song M Y, Yu J S. Enhanced electrocatalytic activity due to additional phosphorous doping in nitrogen and sulfur-doped graphene: A comprehensive study[J]. Carbon, 2014, 78: 257-267.

[37] Xing Z H, Xiao M L, Guo Z L, Yang W S. Colloidal silica assisted fabrication of N,O,S-tridoped porous carbon nanosheets with excellent oxygen reduction performance [J]. Chem. Commun., 2018, 54(32): 4017-4020.

[38] Yang Z, Zhou X M, Jin Z P, Liu Z, Nie H G, Chen X A, Huang S M. A facile and general approach for the direct fabrication of 3D, vertically aligned carbon nanotube array/transition metal oxide composites as non-Pt catalysts for oxygen reduction reactions[J]. Adv. Mater., 2014, 26 (19): 3156-3161.

[39] Sun J, Du L, Sun B Y, Han G K, Ma Y L, Wang J J, Huo H, Du C Y, Yin G P. Bifunctional $LaMn_{0.3}Co_{0.7}O_3$ perovskite oxide catalyst for oxygen reduction and evolution reactions: The optimized e(g) electronic structures by manganese dopant[J]. ACS Appl. Mater. Interfaces, 2020, 12 (45): 24717-24725.

[40] Ren D Z, Ying J, Xiao M L, Deng Y P, Ou J H, Zhu J B, Liu G H, Pei Y, Li S, Jauhar A M, Jin H L, Wang S, Su D, Yu A P, Chen Z W. Hierarchically porous multimetal-based carbon nanorod hybrid as an efficient oxygen catalyst for rechargeable zinc-air batteries[J]. Adv. Funct. Mater., 2020, 30(7): 1908167.

[41] Liu H T, Guan J Y, Yang S X, Yu Y H, Shao R, Zhang Z P, Dou M L, Wang F, Xu Q. Metal-organic framework-derived Co_2P nanoparticle/multi-doped porous carbon as a trifunctional electrocatalyst[J]. Adv. Mater., 2020, 32 (36): 2003649.

[42] Parra-Puerto A, Ng K L, Fahy K, Goode A E, Ryan M P, Kucernak A. Supported transition metal phosphides: activity survey for HER, ORR, OER, and corrosion resistance in acid and alkaline electrolytes[J]. ACS Catal., 2019, 9 (12): 11515-11529.

[43] Liu W W, Ren B H, Zhang W Y, Zhang M W, Li G R, Xiao M L, Zhu J B, Yu A P, Ricardez-Sandoval L, Chen Z W. Defect-enriched nitrogen doped-graphene quantum dots engineered $NiCo_2S_4$ nanoarray as high-efficiency bifunctional catalyst for flexible Zn-air battery[J]. Small, 2019, 15(44): 1903610.

[44] Yu Y D, Zhou J, Sun Z M. Novel 2D Transition-Metal Carbides: Ultrahigh performance electrocatalysts for overall water splitting and oxygen reduction[J]. Adv. Func. Mater., 2020, 30(47): 2000570.

[45] Rasaki S A, Shen H, Thomas T, Yang M. Solid-solid separation approach for preparation of carbon-supported cobalt carbide nanoparticle catalysts for oxygen reduction[J]. ACS Appl. Nano. Mater., 2019, 2(6): 3662-3670.

[46] Huang H T, Chang Y, Jia J C, Jia M L, Wen Z H. Understand the Fe_3C nanocrystalline grown on rGO and its performance for oxygen reduction reaction[J]. Int. J. Hydrogen Energy, 2020, 45(53): 28764-28773.

[47] Wang M, Yang Y S, Liu X, Pu Z H, Kou Z K, Zhu P P, Mu S C. The role of iron nitrides in the Fe-N-C catalysis system towards the oxygen reduction reaction[J]. Nanoscale, 2017, 9(22): 7641-7649.

[48] Tian X L, Wang L, Chi B, Xu Y, Zaman S, Qi K, Liu H, Liao S, Xia B Y. Formation of a tubular assembly by ultrathin $Ti_{0.8}Co_{0.2}N$ nanosheets as efficient oxygen reduction electrocatalysts for hydrogen-/metal-air fuel cells[J]. ACS Catal., 2018, 8(10): 8970-8975.

[49] Kreider M E, Gallo A, Back S, Liu Y, Siahrostami S, Nordlund D, Sinclair R, Norskov J K, King L A, Jaramillo T F. Precious metal-free nickel nitride catalyst for the oxygen reduction raction[J]. ACS Appl. Mater. Interfaces, 2019, 11(30): 26863-26871.

[50] Tian Y H, Xu L, Qiu J X, Liu X H, Zhang S Q. Rational design of sustainable transition metal-based bifunctional electrocatalysts for oxygen reduction and evolution reactions[J]. Sustain.Mater.Techno., 2020, 25: e00204.

[51] Wang M Y, Han B H, Deng J J, Jiang Y, Zhou M Y, Lucero M, Wang Y, Chen Y B, Yang Z Z, N'diaye A T, Wang Q, Xu Z C J, Feng Z X. Influence of Fe substitution into $LaCoO_3$ electrocatalysts on oxygen-reduction activity[J]. ACS Appl. Mater. Interfaces, 2019, 11(6): 5682-5686.

[52] Surendran S, Shanmugapriya S, Sivanantham A, Shanmugam S, Kalai Selvan R. Electrospun carbon nanofibers encapsulated with NiCoP: A multifunctional electrode for supercapattery and oxygen reduction, oxygen evolution, and hydrogen evolution reactions[J]. Adv. Energy Mater., 2018, 8(20): 1800555.

[53] Han X P, Zhang W, Ma X Y, Zhong C, Zhao N Q, Hu W B, Deng Y D. Identifying the activation of bimetallic sites in $NiCo_2S_4$@g-C_3N_4-CNT hybrid electrocatalysts for synergistic oxygen reduction and evolution[J]. Adv. Mater., 2019, 31(18): 1808281.

[54] Liu W W, Ren B H, Zhang W Y, Zhang M W, Li G R, Xiao M L, Zhu J B, Yu A P, Ricardez-Sandoval L, Chen Z W. Defect-enriched nitrogen doped-graphene quantum dots engineered $NiCo_2S_4$ nanoarray as high-efficiency bifunctional catalyst for flexible Zn-air battery[J]. Small, 2019, 15(44): 1903610.

[55] Strickland K, Elise M W, Jia Q Y, Tylus U, Ramaswamy N, Liang W T, Sougrati M T, Jaouen F, Mukerjee S. Highly active oxygen reduction non-platinum group metal electrocatalyst without direct metal-nitrogen coordination[J]. Nat. Commun., 2015, 6: 7343.

[56] Varnell J A, Tse E C M, Schulz C E, Fister T T, Haasch R T, Timoshenko J, Frenkel A I, Gewirth A A. Identification of carbon-encapsulated iron nanoparticles as active species in non-precious metal oxygen reduction catalysts [J]. Nat. Commun., 2016, 7: 12582.

[57] Chen M X, Zhu M Z, Zuo M, Chu S Q, Zhang J, Wu Y, Liang H W, Feng X L. Identification of catalytic sites for oxygen reduction in metal/nitrogen-doped carbons with encapsulated metal nanoparticles[J]. Angew. Chem. Int. Ed., 2020, 59(4): 1627-1633.

[58] Chen X Q, Xiao J P, Wang J, Deng D H, Hu Y F, Zhou J G, Yu L, Heine T, Pan X L, Bao X H. Visualizing electronic interactions between iron and carbon by X-ray chemical imaging and spectroscopy[J]. Chem. Sci., 2015, 6(5): 3262-3267.

[59] Hu Y, Jensen J O, Zhang W, Huang Y J, Cleemann LN, Xing W, Bjerrum, N J, Li Q F. Direct synthesis of Fe3C-functionalized graphene by high temperature autoclave pyrolysis for oxygen reduction[J]. ChemSusChem, 2014, 7(8): 2099-2113.

[60] Aijaz A, Masa J, Rsler C, Antoni H, Fischer R A, Schuhmann W, Muhler M. MOF-templated assembly approach for Fe_3C nanoparticles encapsulated in bamboo-like N-doped CNTs: highly efficient oxygen reduction under acidic and basic conditions[J]. Chem. Eur. J., 2017, 23(50): 12125-12130.

[61] Kong A, Zhang Y, Chen Z, Chen A, Li C, Wang H, Shan Y. One-pot synthesized covalent porphyrin polymer-derived core-shell Fe_3C@carbon for efficient oxygen electroreduction [J]. Carbon, 2017, 116: 606-614.

[62] Hu Y, Jensen J O, Zhang W, Cleemann L N, Xing W, Bjerrum N J, Li Q F. Hollow spheres of iron carbide nanoparticles encased in graphitic layers as oxygen reduction catalysts[J]. Angew. Chem. Int. Ed., 2014, 53(14): 3675-3679.

[63] Zhu J B, Xiao M L, Liu C P, Ge J J, St-Pierre J, Xing W. Growth mechanism and active site probing of Fe_3C@N-doped carbon nanotubes/C catalysts: guidance for building highly efficient oxygen reduction electrocatalysts[J]. J. Mater. Chem. A, 2015, 3(43): 21451-21459.

[64] Xiao M L, Zhu J B, Feng L G, Liu C P, Xing W.Meso/Macroporous nitrogen-doped carbon architectures with iron carbide encapsulated in graphitic layers as an efficient and robust catalyst for the oxygen reduction reaction in both acidic and alkaline solutions[J]. Adv. Mater., 2015, 27(15): 2521-2527.

[65] Nandan R, Pandey P, Gautam A. Atomic Arrangement Modulation in CoFe nanoparticles encapsulated in N-doped carbon nanostructures for efficient oxygen reduction reaction[J]. ACS Appl. Mater. Interfaces, 2021, 13 (3): 3771-3781.

[66] Lv C C, Liang B L, Li K X, Zhao Y, Sun H W. Boosted activity of graphene encapsulated CoFe alloys by blending with activated carbon for oxygen reduction reaction [J]. Biosens. Bioelectron., 2018, 117: 802-809.

[67] Liu Y, Wu X, Guo X, Lee K, Sun Q, Li X, Zhang C, Wang Z, Hu J, Zhu Y, Leung M K H, Zhu Z. Modulated FeCo nanoparticle in situ growth on the carbon matrix for high-performance oxygen catalysts[J]. Mater. Today Energy, 2021, 19: 100610.

[68] Hou Y, Cui S M, Wen Z H, Guo X R, Feng X L, Chen J H. Electrocatalysis: Strongly coupled 3D hybrids of N-doped porous carbon nanosheet/CoNi alloy-encapsulated carbon nanotubes for enhanced electrocatalysis[J]. Small, 2015, 11(44): 5939.

[69] Niu L J, Liu G H, Li Y F, An J W, Zhao B Y, Yang J S, Qu D, Wang X Y, An L, Sun Z C. CoNi alloy nanoparticles encapsulated in N-doped graphite carbon nanotubes as an efficient electrocatalyst for oxygen reduction reaction in an alkaline medium[J]. ACS Sustainable Chem. Eng., 2021, 9(24): 8207-8213.

[70] Zhu J B, Xiao M L, Zhang Y L, Jin Z, Peng Z Q, Liu C P, Chen S L, Ge J J, Xing W. Metal-organic framework-induced synthesis of ultrasmall encased NiFe nanoparticles coupling with graphene as an efficient oxygen electrode for a rechargeable Zn-air battery[J]. ACS Catal., 2016, 6 (10): 6335-6342.

[71] Wang Z, Ang J M, Liu J, Ma X, Kong G H, Zhang Y F, Yan T, Lu X H. FeNi alloys encapsulated in N-doped CNTs-tangled porous carbon fibers as highly efficient and durable bifunctional oxygen electrocatalyst for rechargeable zinc-air battery[J]. Appl. Catal. B: Environ., 2019, 263: 118344.

[72] Niu H J, Chen S S, Feng J J, Zhang L, Wang A J. Assembled hollow spheres with CoFe alloyed nanocrystals encapsulated in N, P-doped carbon nanovesicles: An ultra-stable bifunctional oxygen catalyst for rechargeable Zn-air battery[J]. J. Power Sources, 2020, 475: 228594.

[73] Dong Z, Li M X, Zhang W L, Liu Y J, Wang Y, Qin C L, Yu L T, Yang J, Zhang X, Dai X P. Cobalt nanoparticles embedded in N, S Co-doped carbon towards oxygen re-

duction reaction derived by *in-situ* reducing cobalt sulfide[J]. ChemCatChem, 2019, 11(24): 6039-6050.

[74] Qiao B, Wang A, Yang X, Allard L F, Jiang Z, Cui Y, Liu J, Li J, Zhang T. Single-atom catalysis of CO oxidation using Pt_1/FeO_x[J]. Nat. Chem., 2011, 3(8): 634-641.

[75] Lefevre M, Proietti E, Jaouen F, Dodelet J P. Iron-based catalysts with improved oxygen reduction activity in polymer electrolyte fuel cells[J]. Science, 2009, 324(5923): 71-74.

[76] Chen Y J, Ji S F, Wang Y G, Dong J C, Chen W X, Li Z, Shen R A, Zheng L R, Zhuang Z B, Wang D S, Li Y D. Isolated single iron atoms anchored on N-doped porous carbon as an efficient electrocatalyst for the oxygen reduction reaction[J]. Angew. Chem. Int. Ed., 2017, 56(24): 6937-6941.

[77] Zhao X L, Shao L, Wang Z M, Chen H B, Yang H P, Zeng L. *In situ* atomically dispersed Fe doped metal-organic framework on reduced graphene oxide as bifunctional electrocatalyst for Zn-air batteries[J]. J. Mater. Chem. C, 2021, 9(34): 11252-11260.

[78] Zhao X, Shao L, Wang Z, Chen H, Yang H, Zeng L. In situ atomically dispersed Fe doped metal-organic framework on reduced graphene oxide as bifunctional electrocatalyst for Zn-air batteries[J]. J. Mater. Chem. C, 2021, 9 (34): 11252-11260.

[79] Gong X F, Zhu J B, Li J Z, Gao R, Zhou Q Y, Zhang Z, Dou H Z, Zhao L, Sui X L, Cai J J, Zhang Y L, Liu B, Hu Y F, Yu A P, Sun S H, Wang Z B, Chen Z W. Self-templated hierarchically porous carbon nanorods embedded with atomic $Fe-N_4$ active sites as efficient oxygen reduction electrocatalysts in Zn-air batteries[J]. Adv. Funct. Mater., 2021, 31(8): 2008085.

[80] Fu X G, Jiang G P, Wen G B, Gao R, Li S, Li M, Zhu J B, Zheng Y, Li Z Q, Hu Y F, Yang L, Bai Z Y, Yu A P, Chen Z W. Densely accessible $Fe-N_x$ active sites decorated mesoporous-carbon-spheres for oxygen reduction towards high performance aluminum-air flow batteries[J]. Appl. Cata. B: Environ., 2021, 293: 120176.

[81] Xiao M L, Xing Z H, Jin Z, Liu C P, Ge J J, Zhu J B, Wang Y, Zhao X, Chen Z W. Preferentially engineering FeN4 edge sites onto graphitic nanosheets for highly active and durable oxygen electrocatalysis in rechargeable Zn-air batteries[J]. Adv. Mater., 2020, 32(49): 2004900.

[82] Han X P, Ling X F, Wang Y, Ma T Y, Zhong C, Hu W B, Deng Y D. Generation of nanoparticle, atomic-cluster, and single-atom cobalt catalysts from zeolitic imidazole frameworks by spatial isolation and their use in zinc-air batteries[J]. Angew. Chem. Int. Ed., 2019, 58(16): 5359-5364.

[83] Pan Y, Liu S J, Sun K A, Chen X, Wang B, Wu K L, Cao X, Cheong W-C, Shen R A, Han A J, Chen Z, Zheng L R, Luo J, Lin Y, Liu Y Q, Wang D S, Peng Q, Zhang Q, Chen C, Li Y D. A bimetallic Zn/Fe polyphthalocyanine-derived dingle-atom $Fe-N_4$ catalytic site: a superior trifunctional catalyst for overall water splitting and Zn-air batteries[J]. Angew. Chem. Int. Ed., 2018, 57(28): 8614-8618.

[84] Chen G B, Liu P, Liao Z Q, Sun F F, He Y H, Zhong H X, Zhang T, Zschech E, Chen M W, Wu G, Zhang J, Feng X L. Zinc-mediated template synthesis of Fe-N-C electrocatalysts with densely accessible $Fe-N_x$ active sites for efficient oxygen reduction[J]. Adv. Mater., 2020, 32(8): 1907399.

[85] Arif Khan M, Sun C L, Cai J, Ye D X, Zhao K N, Zhang G B, Shi S S, Ali Shah L, Fang J H, Yang C, Zhao H B, Mu S C, Zhang J J. Potassium-ion activating formation of Fe-N-C moiety as efficient oxygen electrocatalyst for Zn-air batteries[J]. ChemElectroChem, 2021, 8(7): 1298-1306.

[86] Ding S C, Lyu Z Y, Sarnello E, Xu M J, Fang L Z, Tian H Y, Karcher S, Li T, Pan X Q, Mccloy J, Ding G D, Zhang Q, Shi Q R, Du D, Li J C, Zhang X, Lin Y H. A MnO_x enhanced atomically dispersed iron-nitrogen-carbon catalyst for the oxygen reduction reaction[J]. J. Mater. Chem. A, 2021, DOI: 10.1039/d1ta07219f.

[87] Cheng Q Q, Yang L J, Zou L L, Zou Z Q, Chen C, Hu Z, Yang H. Single cobalt atom and N co-doped carbon nanofibers as highly durable electrocatalyst for oxygen reduction reaction[J]. ACS Catal., 2017, 7(10): 6864-6871.

[88] Wu G, More K L, Johnston C M, Zelenay P. High-performance electrocatalysts for oxygen reduction derived from polyaniline, iron, and cobalt[J]. Science, 2011, 332(6028): 443-447.

[89] Zhou Q Y, Cai J J, Zhang Z, Gao R, Chen B, Wen G B, Zhao L, Deng Y P, Dou H Z, Gong X F, Zhang Y L, Hu Y F, Yu A P, Sui X L, Wang Z B, Chen Z W. A gas-phase migration strategy to synthesize atomically dispersed Mn-N-C catalysts for Zn-air batteries[J]. Small Methods, 2021, 5(6): 2100024.

[90] Song P, Luo M, Liu X Z, Xing W, Xu W L, Jiang Z, Gu L. Zn single atom catalyst for highly efficient oxygen reduction reaction[J]. Adv. Funct. Mater., 2017, 27(28): 1700802.

[91] Zhang S A, Xue H, Li W l, Sun J, Guo N K, Song T S, Dong H L, Zhang J W, Ge X, Zhang W, Wang Q. Constructing precise coordination of nickel active sites on

hierarchical porous carbon framework for superior oxygen reduction[J]. Small, 2021, 17(35): 2102125.

[92] Shang H S, Zhou X Y, Dong J C, Li A, Zhao X, Liu Q H, Lin Y, Pei J J, Li Z, Jiang Z L, Zhou D N, Zheng L R, Wang Y, Zhou J, Yang Z K, Cao R, Sarangi R, Sun T T, Yang X, Zheng X S, Yan W S, Zhuang Z B, Li J, Chen W X, Wang D S, Zhang J T, Li Y D. Engineering unsymmetrically coordinated Cu-S_1N_3 single atom sites with enhanced oxygen reduction activity[J]. Nat. Commun., 2020, 11: 3049.

[93] Liang H W, Zhuang X D, Bruller S, Feng X L, Mullen K. Hierarchically porous carbons with optimized nitrogen doping as highly active electrocatalysts for oxygen reduction[J]. Nat. Commun., 2014, 5: 4973.

[94] Li Z Q, Jiang G P, Deng Y P, Liu G H, Ren D Z, Zhang Z, Zhu J B, Gao R, Jiang Y, Luo D, Zhu Y F, Liu D H, Jauhar A M, Jin H L, Hu Y F, Wang S, Chen Z W. Deep-breathing honeycomb-like Co-N_x-C nanopolyhedron bifunctional oxygen electrocatalysts for rechargeable Zn-air batteries[J]. iScience, 2020, 23(8): 101404.

[95] Guo C X, Zheng Y, Ran J R, Xie F X, Jaroniec M, Qiao S Z. Engineering high-energy interfacial structures for high-performance oxygen-involving electrocatalysis [J]. Angew. Chem. Int. Ed., 2017, 56(29): 8539-8543.

[96] Lin Y X, Yang L, Zhang Y K, Jiang H L, Xiao Z J, Wu C Q, Zhang G B, Jiang J, Song L. Defective carbon-CoP nanoparticles hybrids with interfacial charges polarization for efficient bifunctional oxygen electrocatalysis[J]. Adv. Energy Mater., 2018, 8(18): 1703623.

[97] Zhu J B, Xiao M L, Li G R, Li S, Zhang J, Liu G H, Ma L, Wu T P, Lu J, Yu A P, Su D, Jin H L, Wang S, Chen Z W. A triphasic bifunctional oxygen electrocatalyst with tunable and synergetic interfacial structure for rechargeable Zn-air batteries[J]. Adv. Energy Mater., 2020, 10(4): 1903003.

[98] Niu Y, Xiao M L, Zhu J B, Zeng T T, Li J D, Zhang W Y, Su D, Yu A P, Chen Z W. A “trimurti” heterostructured hybrid with an intimate CoO/Co_xP interface as a robust bifunctional air electrode for rechargeable Zn-air batteries [J]. J. Mater. Chem. A, 2020, 8(18): 9177-9184.

[99] Yin H, Zhang C Z, Liu F, Hou Y L. Hybrid of iron nitride and nitrogen-doped graphene aerogel as synergistic catalyst for oxygen reduction reaction[J]. Adv. Funct. Mater., 2014, 24(20): 2930-2937.

[100] Dong Y Y, Deng Y J, Zeng J H, Song H Y, Liao S J. A high-performance composite ORR catalyst based on the synergy between binary transition metal nitride and nitrogen-doped reduced graphene oxide[J]. J. Mater. Chem. A, 2017, 5(12): 5829-5837.

[101] Xiao M L, Zhang H, Chen Y T, Zhu J B, Gao L Q, Jin Z, Ge J J, Jiang Z, Chen S L, Liu C P, Xing W. Identification of binuclear Co_2N_5 active sites for oxygen reduction reaction with more than one magnitude higher activity than single atom CoN_4 site[J]. Nano Energy, 2018, 46: 396-403.

[102] Xiao M L, Chen Y T, Zhu J B, Zhang H, Zhao X, Gao L Q, Wang X, Zhao J, Ge J J, Jiang Z, Chen S L, Liu C P, Xing W. Climbing the apex of the ORR volcano plot via binuclear site construction: electronic and geometric engineering[J]. J. Am. Chem. Soc., 2019, 141(44): 17763-17770.

[103] Xiao M L, Zhu J B, Li S, Li G R, Liu W W, Deng Y P, Bai Z Y, Ma L, Feng M, Wu T P, Su D, Lu J, Yu A P, Chen Z W. 3D-Orbital occupancy regulated Ir-Co atomic pair towards Superior bifunctional oxygen electrocatalysis[J]. ACS Catal., 2021, 11(14): 8837-8846.

[104] Jin Z Y, Li P P, Meng Y, Fang Z W, Xiao D, Yu G H. Understanding the inter-site distance effect in single-atom catalysts for oxygen electroreduction[J]. Nat. Catal., 2021, 4(7): 615-622.

[105] Luo F, Zhu J B, Ma S X, Li M, Xu R Z, Zhang Q, Yang Z H, Qu K G, Cai W W, Chen Z W. Regulated coordination environment of Ni single atom catalyst toward high-efficiency oxygen electrocatalysis for rechargeable zinc-air batteries[J]. Energy Storage Mater., 2021, 35: 723-730.

碱性介质中非贵金属氧还原催化剂的结构调控进展

王 雪[1,2],张 丽[1],刘长鹏[1,2],葛君杰[1,2],
祝建兵[1,2*],邢 巍[1,2*]

(1. 中国科学院长春应用化学研究所电分析化学国家重点实验室,吉林 长春 130022;
2. 中国科学技术大学,安徽 合肥 230026)

摘要: 碱性介质中的氧还原反应是金属-空气电池和阴离子交换膜燃料电池的重要电化学过程。但是,其动力学缓慢,因而引起了对高效电催化剂的广泛研究。其中,非贵金属催化剂可有效地规避铂基催化剂成本和储量的问题,而备受关注。但其挑战在于将性能提高到可与 Pt 基催化材料媲美。鉴于非贵金属催化剂的组成和结构对催化性能有着至关重要的影响,精准地调控催化剂的结构有望消除非贵金属催化剂和商业铂基催化剂的活性差距。在该评述中,我们致力于总结通过结构调控来提升性能的研究进展。我们首先介绍了四种极具代表性的非贵金属催化剂,包括非金属碳基材料、金属化合物、石墨化碳层包覆金属颗粒、原子分散的金属-氮-碳材料,突出了催化活性位点和催化机理。随后,针对于这些催化剂,我们归纳了从微纳尺度到原子层面的结构调控策略,如分级多孔结构的设计、界面工程、缺陷工程以及原子对活性位点的构建。我们着重讨论了结构和性能之间的依赖关系。从加速传质、增加可及的活性位点数量、可调控的电子状态和多组分之间的协同效应,讨论了这些结构变化引起的活性改进的起源。最后,我们对该领域存在的挑战以及未来的前景进行了展望。

关键词: 氧气还原反应;非贵金属催化剂;结构调控